-

Scientific - Technical Report

(2018 - 2020)

Competition:	**Complex Ground-Breaking Research Projects_PCCF 2016**
No. of the contract:	PCCF18/2018
Research domain:	Engineering sciences
Title:	High-k Nanoparticle Multilayer Dielectrics for Nanoelectronics and Energy Storage Applications
Acronym:	HIGHkDEVICE
Duration (months):	48 months
Total funded budget:	8.500.000,00 Ron
- 2018 settled	531.429,00 Ron
- 2019 settled	2.125.000,00 Ron
- 2020 settled	2.125.000,00 Ron
Project web page:	http://nanomat.usv.ro/pagina-05-5-a.php
Host institution:	Universitatea "Ștefan cel Mare" din Suceava
Project manager	Aurelian ROTARU
Project partner 1 (P1): Universitatea „Alexandru Ioan Cuza”, Iasi	Liliana MITOȘERIU
Project partner 2 (P2): Institutul National de Cercetare Dezvoltare pentru Fizica Materialelor	Ioana PINTILIE
Project partner 3 (P3): Institutul National de Cercetare Dezvoltare pentru Fizica Laserilor, Plasmei si Radiatiei	Aurelian MARCU

Summary for publication.

1. Summary of the context and overall objectives of the project (for the 2018-2020 period, include the conclusions of the action)

It should preferably not exceed two pages of a text document. This part must not contain any confidential data.
Beside the summary filled within the tool, diagrams or photographs illustrating and promoting the work of the project can be provided (only as images)

The main goal of HIGHkDEVICE project is to rationally integrate solution-processable, monodisperse perovskite pristine and doped $BaTiO_3$ nanocrystals into high quality, close-packed dielectric films with controlled thickness and tunable dielectric properties (high dielectric breakdown field strength, low leakage current and low interface trap density), which can be integrated into solid state electronic devices, such as flexible capacitors and field effect transistors (FET).

We would like at this point, underlining that, due to the budget modifications imposed by the founding agency (UEFISCDI), the research activities presented in the original (English) version of the proposal (4 "thrusts" with 23 research activities) have been extended into Romanian version of the Research plan (4 "thrusts" with 45 research activities). Although the research tasks listed in these two versions of the proposal/research plan are generally similar, there are some slight differences between them. ***Therefore, the work performed in this project generally followed the task/activities agreed with the funding agency. These are listed in the specific Realization Plan, accessible via the UEFISCDI Platform.***

In the first half of this project, the research activities were mainly focused on the: ***(i)*** synthesis, characterization, testing and optimization of the properties of thin dielectric layers containing colloidal $BaTiO_3$ nanoparticles, as well as the development of strategies for functionalization of $BaTiO_3$ nanoparticles as a dense and continuous thin layer; ***(ii)*** the study of the influence of size effects and the nature of the capping agents on the ferroelectric properties of differently-sized $BaTiO_3$ cuboidal nanocrystals by using neutron diffraction techniques; ***(iii)*** exploring the infiltration of nanoparticle layers with a low molecular weight monomer and initiating the *in-situ* polymerization process and characterizing the resulting dielectric layers; ***(iv)*** the advanced characterization of the dielectric and piezoelectric properties of individual pristine and $BaTiO_3$ cuboidal nanoparticles by using in-situ transmission electron microscopy (TEM) in tandem with piezoresponse force microscopy (PFM) techniques; **(v)** the study of the structural, morphological, and compositional characterization of $BaTiO_3$ nanopowders and the measurement of their dielectric and ferroelectric properties; **(vi)** the use of $BaTiO_3$ colloidal nanocrystals for the design of ferroelectric inks and as building blocks for the design of nanoparticle-based dielectric and ferroelectric films; **(vii)** fabrication of pellets using nanoparticle-based powders and the densification of these pellets by using a spark plasma sintering method to improve their porosity and dielectric response; **(viii)** the comprehensive dielectric characterization of the nanopowders by using dielectric spectroscopy

and piezoresponse force microscopy; **(ix)** the use of $BaTiO_3$ colloidal nanoparticles as building blocks for the rational design of polymer-ceramic nanocomposite films and membranes and their integration into capacitor devices and the characterization and optimization of the performance of these capacitors; integration of the dielectric nanopowders into spinel-perovskite magnetoelectric nanocomposites with different architectural complexity (3-3 and 2-2) and the characterization and optimization of the magnetoelectric effect.

The research performed exploited the unique solution-based batch-synthetic route developed by our group for the preparation of aggregate-free monodisperse ferroelectric $ATiO_3$ (A=Ba, Sr) nanocubes with precisely controlled sizes and shapes. Second, this project capitalized on our ability to engineer the surface composition of colloidal nanocrystals via ligand exchange processes, which enabled us to fabricate highly stable solutions by suspending the nanocrystals in both polar and non-polar solvents. The as-prepared colloidal nanocrystals have been individually passivated with oleic acid molecules, which prevent their aggregation and render them dispersible in non-polar solvents, a key requirement in the fabrication of the dielectric inks. Thus, several series of dielectric nanoparticles have been synthesized with controlled sizes and morphologies (cubic, spheres) to tune their dielectric properties and integrated into rigid and flexible electronic devices. *One of the most important outcomes of the research performed to this stage is the fact that our initial findings that the $BaTiO_3$ nanocrystals present an acentric structure (presumably tetragonal, as indicated by the results obtained by the USV, UAIC and NIMP teams in the consortium by using different laboratory techniques, such as conventional X-Ray diffraction, Raman spectroscopy, piezoresponse force microscopy and measurement of the ferroelectric properties) were confirmed by temperature-dependent neutron diffraction techniques, performed through a collaboration with the Oak Ridge national laboratory*. Interestingly, the real crystal structure of the nanocrystals appears to be orthorhombic, and not tetragonal, structure which is also ferroelectric being associated with the off-center shift of the Ti^{4+} within the TiO_6 octahedra, which could lead to high values of the dielectric constant and a robust ferroelectric behavior. In conclusion, all the objectives planned to be achieved at this stage of research have been 100% achieved, the results obtained being very promising in carrying out the subsequent activities provided in the project.

Thus, the entire consortium already published 9 ISI papers and other 6 ISI papers have been already submitted for evaluation. The scientific results obtained into the project have been presented in 15 national and international conferences.

2. Work performed from the beginning of the project to the end of the period covered by the report and main results achieved so far

2.1 Elaboration of strategies for the functionalization of $BaTiO_3$ nanoparticles and their assembly on flat surfaces in dense and orderly thin layer type structures.

A constant effort during the two years of the project was to fabricate $BaTiO_3$ colloidal nanocrystals with different sizes and surface composition (Thrust 1) by using a highly reliable, low cost solvothermal technique and the optimization of the reaction conditions in order to improve the size distribution of the resulting nanocrystals. first step we focused on the optimization of the synthesis conditions of $BaTiO_3$ nanoparticles with cuboidal shape. For this purpose, a systematic study of the role played by different factors (solvent polarity, reaction time, reaction temperature, molar ratio between precursors, solvent and passivation agent, etc.) on the morphology of nanoparticles was performed. We have shown that a rigorous control of the polarity of the solvent allows the stabilization of $BaTiO_3$ nanoparticles with a spherical and cubic shape. The optimum reaction temperature was identified as being 180 ^oC to obtain $BaTiO_3$ nanocubes, while the variation of the reaction time from 24 to 96 hours allowed the control of the size of these nanocubes, which can thus be varied between 5 nm and 160 nm. A diagram of the main steps in the process of nanoparticle synthesis by the solvothermal method is presented in Figure 1. Data obtained by laboratory powder X-ray diffraction (XRD) showed that $BaTiO_3$ nanopowders have a high crystallinity, despite the relatively low synthesis temperature and do not contain impurities (sometimes a small amount of $BaCO_3$ has been detected dur to the high reactivity of Ba^{2+} on the surface of the nanoparticles towards atmospheric CO_2, but this can be removed upon washing the powders with dilute acetic acid). The crystal structure of the powders cannot be accurately identified by interpreting conventional laboratory X-ray diffractograms, even using structural modeling by the Rieveld method. *Structural characterization by laboratory X-ray diffraction was performed by the USV, UAIC and NIMP partners and is currently ongoing. Absent a priori knowledge about the internal structure of the $BaTiO_3$ nanoparticles and the influence of size effects on their crystal lattice, we employed two models were used to perform structural analysis by the Rietveld method, namely the cubic structure (space group Pm3m) and the tetragonal lattice (space group P4mm), respectively.* The

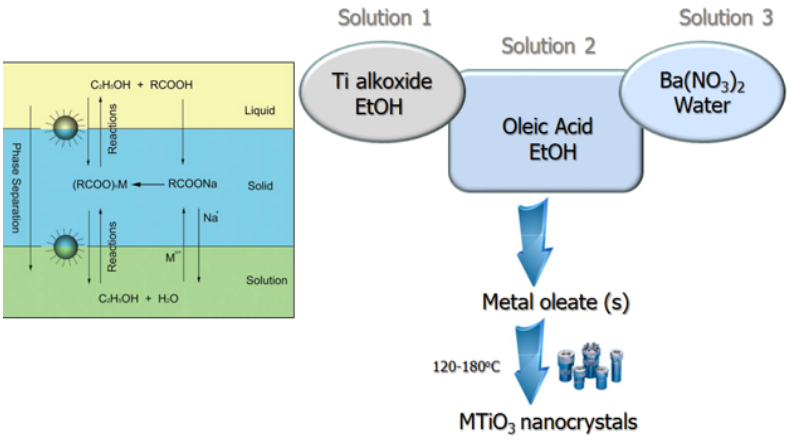

Figure 1. Schematic representation of the synthesis process of perovskite-type nanocrystals using a solvothermal method.

results obtained by conventional X-Ray diffraction and structure refinements (Fullprof software) cannot unambiguously evidence the existence of an off-center shift of the Ti^{4+} within the TiO_6 octahedra associated with the existence of local dipoles. This is because the splitting of the (002) peak at 45° in 2θ associated with the tetragonal phase is obscured in the case of nanoparticle-based powders due the peak broadening associated with the small crystallite size. The figures below represent calculated and experimental XRD patterns of a sample containing 15 nm BTO nanoparticles obtained from refining the structure by the Rietveld method using both the cubic and tetragonal symmetry), thereby indicating the possible existence of a structural tetragonal distortion of the unit cell. As seen in Figure 2, the structural determination suggested that a better fit between the experimental (red curves) and the simulated ones (black curve) is observed and better values of the reliability factors were obtained when a tetragonal unit cell was used (R_p=4,75%, R_{wp}=5.92, χ2=1.88).

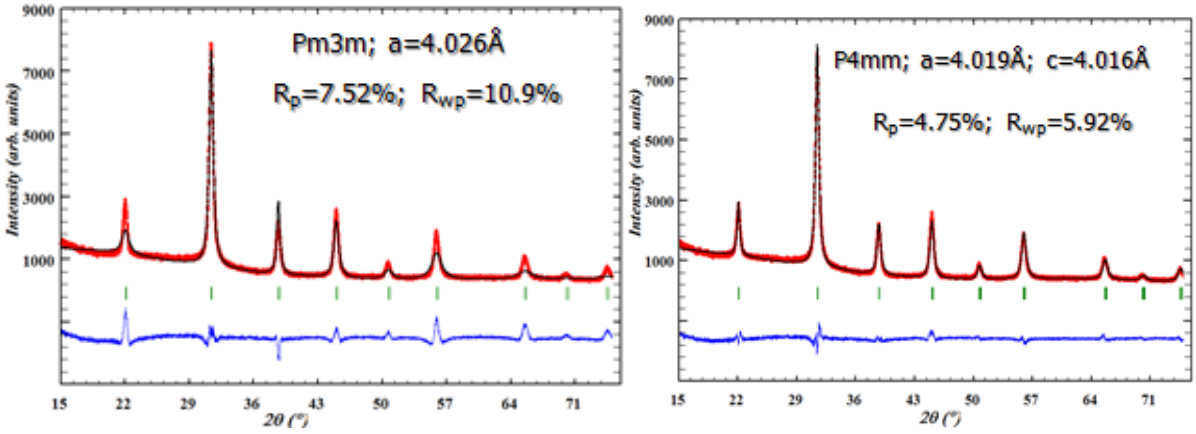

Figure 2. Schematic representation of the synthesis process of perovskite-type nanocrystals using a solvothermal method **(left)**; Raman spectra recorded at different temperatures on $BaTiO_3$ nanocubes with a size of 15 nm (right).

Similar calculations were performed on $BaTiO_3$ nanopowders obtained from hydrothermally prepared spherical nanoparticles with an average size of 60 nm. For these samples, the XRD analysis indicated a pseudo-cubic symmetry (Pm3m spatial group) with unit cell parameters of a=b=c=4.02(3) Å (JCP-PDF File No. 01-074-1963)) and a theoretical density of 5.955g/cm^3. These pseudo-cubic nanopowders were used to produce a set of $BaTiO_3$ thick ceramic films with various grain sizes subjected to a thermal treatment at different temperatures. A superposition of tetragonal and orthorhombic polymorphs with variable amounts was observed at room temperature (Figure 3). It is important to note that such analysis is relevant since the heat treatment of the nanopowders (obtained from a different synthetic approach) will lead to their densification along with a substantial increase of the size of the grains, thereby eliminating the peak broadening process (peaks are much sharper in the second series of powder X-ray diffraction patterns presented). As such, the peak splitting associated with a presumptive tetragonal distortion could be better detected. However, the literature data suggests that most high temperature annealing processed stabilize the cubic polymorph. A very interesting observation is that **the phase composition is also sensitive to the**

influence of external electric fields. For example, for a given sample, it was demonstrated that phase composition and unit cell parameters measured in remanence can be modified by poling at room temperature (under a dc field of 10 kV/cm for 10 minutes, at room temperature and then the field removed and XRD patterns collected in remanence).

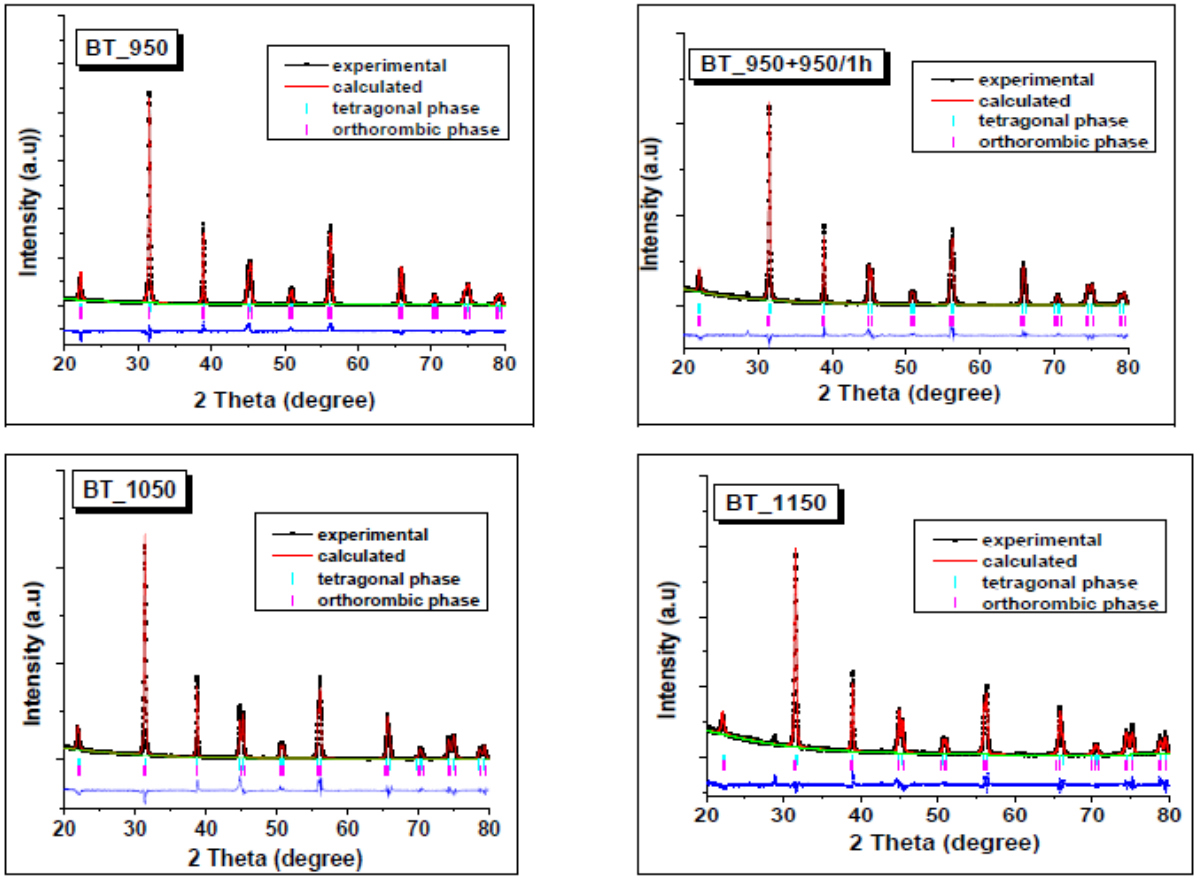

Figure 3. Calculated and experimental XRD patterns of a sample containing 15 nm BTO nanoparticles obtained from refining the structure by the Rietveld method using both the cubic and tetragonal symmetry).

Since the assessment of a tetragonal distortion in $BaTiO_3$ nanostructures from conventional X-Ray diffraction experiments remains elusive, results were not presented in the report and temperature-dependent Raman spectroscopy measurements are described, instead (see Section 2, Figure 1 in the Technical Report). These measurements suggest that, at least at a local scale, an acentric structure is present in the $BaTiO_3$ nanostructures, associated with the existence of ferroelectricity and possibly associated with high dielectric constant values since the Curie temperature in these nanostructures should be close to room temperature, due to the influence of the surface effects.

To further elucidate the crystal structure of the BTO nanopowders we exploited a unique opportunity to perform neutron diffraction experiments at the Oak Ridge National Laboratory (USA) on surface engineered BTO nanoparticles passivated with both nonpolar and polar ligands. The local-average correlation length scales determined experimentally evidenced for the first time the existence of a rhombohedral structure (space group R3m), in $BaTiO_3$ nanocubes, undetectable by conventional X-Ray

diffraction techniques. The existence of the rhombohedral distortion in 10 nm BTO nanocubes was ascribed to increased dipole-dipole correlations in small nanoparticles, enhanced by the presence of a polar ligand on the surface of the perovskite nanocrystals. As a result of this international collaboration, a manuscript was accepted by Chemistry-A European Journal, in March 2021 (https://doi.org/10.1002/chem.202100692). It is worth mentioning that *Landau-based calculations of free energy dependence as a function of the grain size in $BaTiO_3$ performed by the UAIC team provided a generalized grain size-temperature phase diagram of $BaTiO_3$. This is represented in Figure 4, whereby the weights of the rhombohedral (R), orthorhombic (O), tetragonal (T) and cubic (C) polymorphs are represented in colour scale and the black lines are characterized by the same free energy minimum in two phases) indicated that at such small scale, co-existence of more polymorphs is likely around room temperature.*

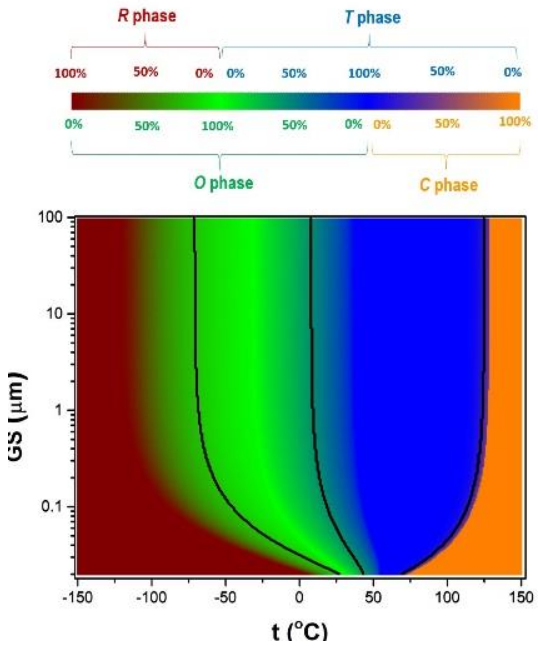

Figure 4. Landau-based calculations of free energy dependence as a function of the grain size in $BaTiO_3$.

To elucidate the local structural distortions existing in the $BaTiO_3$ colloidal nanocrystals have been studied by room temperature Raman spectroscopy. It is well-known that in cubic $BaTiO_3$ (space group Pm3m) the perfectly symmetrical coordination environment around the Ti^{4+} ions is associated with the $3F_{1u}+F_{2u}$ phonons, which correspond to Raman inactive modes. However, when the titanium centers undergo a off-center shift, the symmetry of the lattice will be lowered to tetragonal (space group P4mm), thereby giving rise to Raman active phonons represented by $3[A_1(TO)+A1(LO)]+B_1+4[E(TO)+E(LO)]$. As seen in Figure 5, the low temperature (T=10- 130 ^oC) Raman spectra of 15 nm $BaTiO_3$ nanocrystals feature well-defined bands located around 192, 262, 311, 529 and 720 cm^{-1}. These bands have been assigned to the $E(2(TO)+E(1LO)+A_1(TO)+A1(LO)$, $A_1(2TO)$, $E(3TO)+E_2(LO)+B_1)$, $E(4TO)+A_1(3TO)$ and $E(4LO)+A_1(3LO)$ Raman modes, thereby indicating the presence of local tetragonal distortions in the corresponding nanopowdered samples. It is worth noting that the bands at 311 and 720 cm^{-1}, which are generally considered the signature of the tetragonal structure, are well-defined and relatively strong in intensity. Furthermore, the Raman bands were found to broaden with decreasing the size of the nanocrystals from 35 to 5 nm, which indicate that the tetragonal distortion is accompanied by a notable decrease of the structural coherence as the nanoparticle size decreases in perovskite nanocrystals. Upon increasing temperature to 150 ^oC the Raman peaks do not disappear completely, indicating a phase transition tetragonal to cubic, as expected in bulk $BaTiO_3$. Instead, the Raman bands broaden and their intensity decrease significantly, which suggest that the tetragonal-cubic phase transition occurs, but is diffuse and although at

high temperature most of the $BaTiO_3$ nanocrystals are cubic, some pockets in which the tetragonal distortion is preserved still exist in the material.

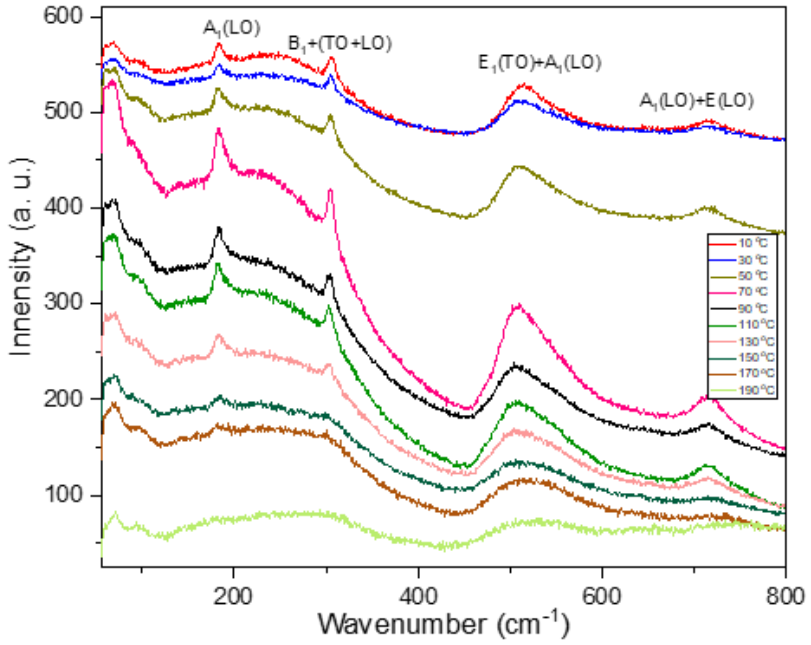

Figure 5. Raman spectra of 15 nm $BaTiO_3$ nanocubes recorded at different temperatures.

TEM images presented in Figure 6 reveal the morphology and crystallinity of $BaTiO_3$ nanocubes obtained under different reaction conditions. Nanocubes are nearly monodisperse and present an average edge length which can be varied from 5±1 nm to 160±2 nm, respectively.

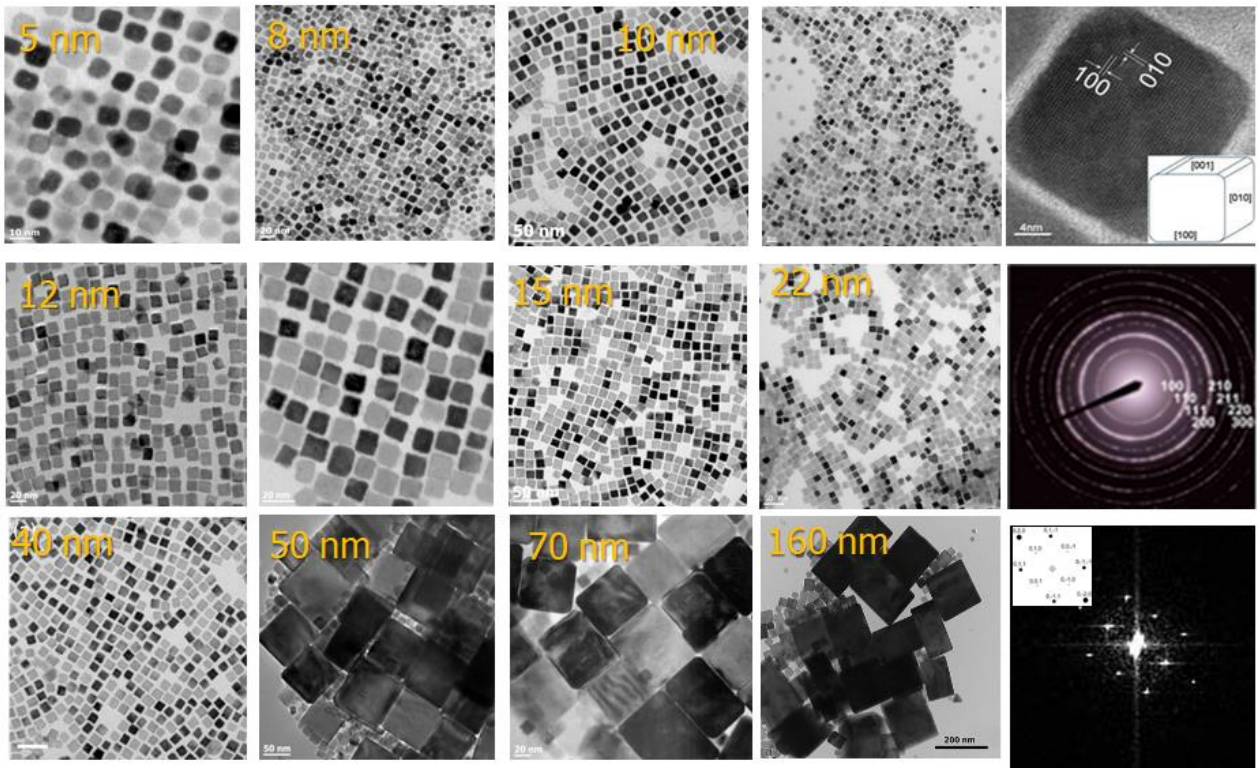

Figure 6. TEM micrographs of $BaTiO_3$ nanocubes synthesized at 180 °C by varying the polarity of the reaction medium and the reaction time (from 48 to 96 hours).

The nanoparticles are well-separated due to the retention of oleic acid molecules on the surface of each individual nanocrystal which enable the nanoparticles to organize on planar surfaces with the formation of self-assembled monolayers. The HRTEM image of an individual 10 nm $BaTiO_3$ nanocube (top right image) reveals a uniform contrast across the nanoparticle indicating a high crystallinity, despite the relatively low reaction temperature.

The lattice fringes observed by HRTEM corresponds to an interplanar distance of 4.09Å, and was ascribed to the {001} family of planes. It is worth mentioning that the retention of oleic acid molecules on their surfaces renders the as-prepared $BaTiO_3$ nanocrystals highly dispersible in non-polar solvents such as toluene or hexane. This will not only prevent the aggregation of the nanoparticles, but also makes them hydrophilic and dispersible in non-polar solvents with formation of very stable colloidal solutions (inks), which can be used for the deposition of nanoparticle-based films upon solution casting followed by the controlled evaporation of the solvent. The existence of oleic acid molecules chemisorbed on the surface of the nanoparticles was confirmed experimentally FT-IR spectra spectroscopy analysis of neat oleic acid and oleic 15 nm $BaTiO_3$ nanocubes. The precise control over the shape, size and surface composition of the perovskite nanocubes in combination with an evaporation-induced self-assembly process allowed us to use the colloidal nanocrystals as building blocks for the design of mesoscale hierarchical structures, such as 3D superlattice assemblies and superparticles. Such systems are attractive from both a fundamental and technological viewpoint, including the study of dipole-dipole interactions in ferroic or multiferroic systems or in the design of novel mesoscale functional materials/nanocomposites. with potential applications in energy conversion and data storage. Superlattice structures of $BaTiO_3$ nanocubes can be easily obtained by casting a 0.1 M solution onto different substrates, such as TEM copper grids or silicon wafers followed by the slow evaporation of the solvent, whereby the nanocrystals rearrange into highly ordered, densely packed 3-D configurations. The visual inspection of the substrates reveals the formation of nanoparticle layers with rainbow-like appearance, which is strongly indicative of the formation of long range ordered arrays of nanocrystals *To ascertain the crystal structure of $BaTiO_3$ nanocrystals powders, high resolution TEM analysis was performed by NIMP partner.* The samples analyzed were provided by the USV team or were prepared in-house, using the synthesis facilities available at NIMP. These samples were characterized by temperature dependent X-

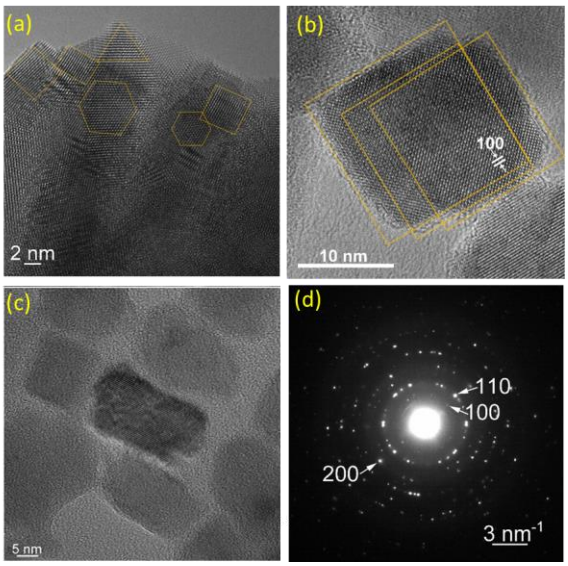

Figure 7. TEM images of the nanocubes (NC). High magnification view of not dispersed particles in ethanol (a); high magnification views of partially dispersed (b) and completely/entirely dispersed in cyclohexane (c), and the corresponding SAED diagram (d). The faint lines are drawn for eye guiding.

ray diffraction measurements, in conjunction with TEM and Raman measurements. Representative TEM images corresponding to these samples are presented in Figures 7 and 8 whereas the data obtained from the fitting of the powder X-ray diffraction patterns of these samples by using the Pawley method are presented in Table 1. As seen in the TEM micrographs, the $BaTiO_3$ nanoparticles are cuboidal in shape, they have an average edge length of about 10-12 nm and are well separated, which confirms their high quality and the reproducibility of the synthetic approach.

The Pawley method is a whole powder pattern decomposition procedure which was adopted to perform unit cell refinements and calculate the size of the crystallites which cat as scattering centers for the X-Ray radiation (Cu K_α) and the microstrain of the powdered samples, respectively. of the $BaTiO_3$ samples investigated. Unlike the Rietveld method, in the Pawley's approach the intensities are considered as refinable parameters, which complements the experimental results obtained from structure refinements by using the traditional Rietveld method. The features observed in XRD patterns, especially the anisotropic line broadening, seems to be qualitatively explained by assuming the presence of a surface relaxation effect, as depicted in the following figure.

Table 1. Unit cell parameters, crystallite size and microstrain values of commercial and nanoscale $BaTiO_3$ samples prepared by the NIMP team

Sample	Synthesis Method	Crystal structure	Crystallite size (nm) Min-Max*	Microstrain (arb.units)	Lattice constant (Å)
BTOm	Commercial	Tetragonal	118	0.16	a = 3.996 c = 4.032
BTO1		Cubic	10.1 9.3 ÷ 13.2	0.64	4.022
BTO3	HT	Cubic	18.0 17.8 ÷ 23.3	0.24	4.026
BTO18	HT	Cubic	23.9 22.9 ÷ 31.7	0.29	4.025

* The minimum values were obtained upon fitting by using the TOPAS softare without considering the microstrain, the maximum values being obtained by considering anisotropic microstrain.

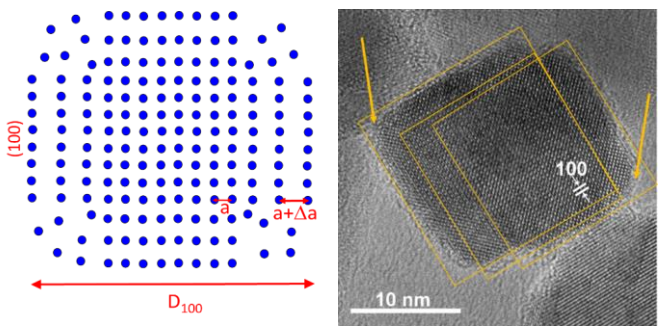

Figure 8. Sketch of surface relaxation in nanocubes, drawn with/for exaggerated relaxation (a), and TEM micrograph showing cubes with beveled/rounded corners (b).

BTOm is the name of a micrometer-sized size, whereas BTO1, BTO2 and BTO3 stand for nanometer- size samples obtained by solvothermal method with different processing times. In conclusion, it was found that the structure is more-likely distorted cubic with large microstrain, with no evidence of a ferroelectric phase transition up to 140 °C. *However, we should emphasize that powder X-*

Ray diffraction techniques provide a limited information about phase transition in titanium-containing perovskites, since such transitions are diffuse in temperature and have a mixed character (displacive and order-disorder). Anisotropic lattice distortions are revealed by XRD analysis which can be interpreted as surface relaxation. *These experimental results will be included into a joint paper between USV, UAIC and NIMP partners.*

The existence of oleic acid molecules chemisorbed on the surface of the nanoparticles was confirmed experimentally FT-IR spectra spectroscopy analysis of neat oleic acid and oleic 15 nm $BaTiO_3$ nanocubes. The corresponding spectra indicated strong similarities between the absorption bands appearing at 3007 cm^{-1} specific to the stretching mode of the =C–H bond and those at 2934, 2854, 2924 and 2845 cm^{-1}, associated with the C-H (ν_{asym} and ν_{sym}) stretching modes of the long aliphatic chains (Figure 9). The band located at 1714 cm^{-1} in the FTIR spectrum of oleic acid, corresponding to the –C=O stretching mode, is found to be shifted to higher wave numbers in the spectrum of the as-prepared 15 nm $BaTiO_3$ nanoparticles because of the conversion of the carboxyl group into carboxylate COO^- ions and their subsequent coordination to the metal centers on the surface of the nanocrystals. The carboxylate ions are also associated with the bands at 1541 and 1454 cm^{-1} (ν_{asym} and ν_{sym}), whereas the bands at 1089 and 904 cm^{-1} have been assigned to the CO vibration in ethers and the scissoring vibration (δ') of the CH_2 group, respectively. A key step in the design of nanoparticle-based devices, such as capacitors[45], field effect transistors[46], inverters[47], integrated circuits[48] or bipolar resistive switching memories[49] is the design of uniform, defect-free nanocrystal-based thin films with tunable thickness on various substrates. The high quality of the perovskite cuboidal nanocrystals, as well as their ability to be dispersed into non-polar solvents allowed us to fabricate uniform and crack-free ferroelectric films on large surfaces by an evaporative-driven assembly process. The further annealing of these films will eliminate the intercrystal void spaces resulting from the compact assembly of the nanocrystals and densify the films, thereby making perovskite nanocubes very promising for implementation in flexible electronics. Thermal analysis experiments indicated that the amount of oleic acid molecules retained at the surface of the $BaTiO_3$ cuboidal nanocrystals decreases from

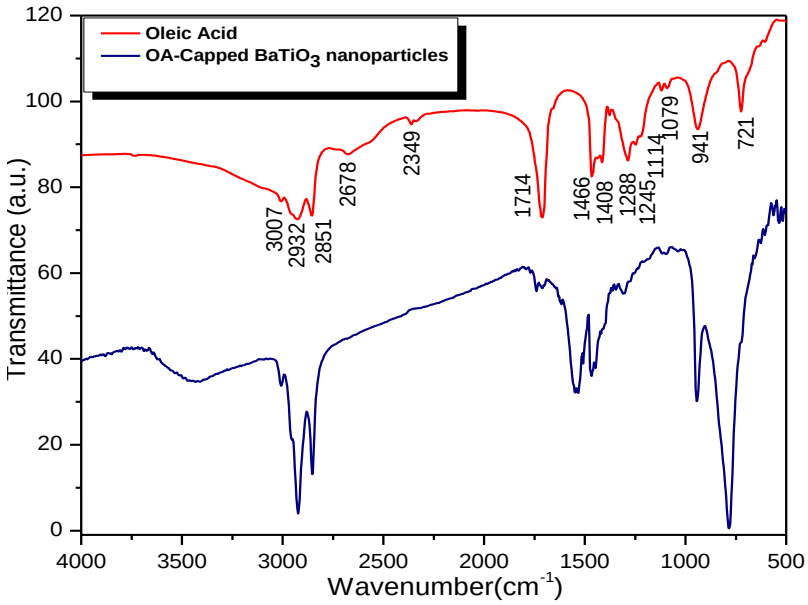

Figure 9. FTIR spectrum of neat oleic acid and oleic acid capped 15 nm $BaTiO_3$ nanoparticles.

9.1% to 4.1% with increasing the particle size from 5 to 40 nm as a result of the decrease of the surface-to-volume ratio of the nanoparticles with increasing their average edge length.

2.2. Fabrication of Dielectric and Semiconductor Inks by Using Variable Sized $BaTiO_3$ Colloidal Nanocrystals

The retention of oleic acid molecules on the surface of the BaTiO3 colloidal nanocrystals makes them amenable to suspension into non-polar solvents, such as toluene and hexane, with the formation of highly stable colloidal solutions, which can be used as inks for the fabrication of dielectric films upon solution casting and controlled evaporation of the solvent. It is worth noting that small nanocrystals possess an increased solubility in non-polar solvents compared with those reported previously in the literature with values of the solubility as high as 150 mg/mL for 15 nm nanocrystals. Furthermore, we demonstrated the surface engineering is very versatile in the case of these nanomaterials by rendering oleic acid capped $BaTiO_3$ nanocubes hydrophilic and dispersible into polar solvents via sequential ligand exchange chemistry with nitrosonium tetrafluoroborate ($NOBF_4$) yielding highly stable colloidal solutions in polar solvents, such as dimethyl formamide.

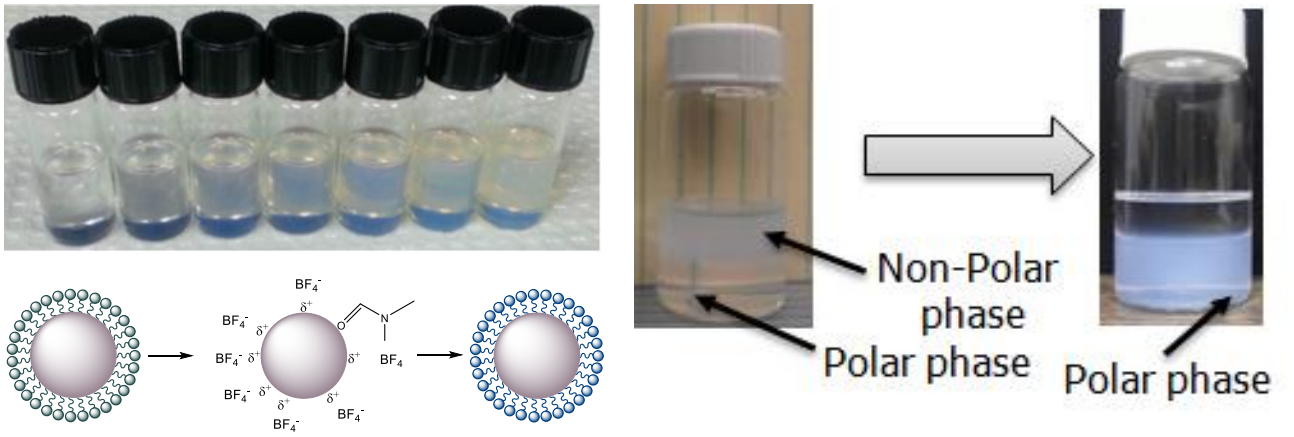

Figure 10. 15 nm $BaTiO_3$ nanoparticle-based inks with different concentrations; the schematic of the ligand exchange process in which nonpolar oleic acid molecules chemisorbed on the surface of each individual nanocube are exchanged with BF_4^- ions, rendering the nanocubes hydrophilic. Right image, the mixture of polar and nonpolar phases showing $BaTiO_3$ nanocrystals passing from the nonpolar solvent into the polar phase.

Therefore, it can be clearly seen that after the ligand exchange process, the initially hydrophobic $BaTiO_3$ nanocubes suspended in toluene (top phase in the left vial) are found as the bottom phase of the mixture containing the colloidal nanocrystals and dimethyl formamide (right vial). As anticipated, the $BaTiO_3$ colloidal nanocrystals can be used for the fabrication of inks which will be subsequently used in the fabrication of thin films. Similarly, semiconducting nanocrystals, such as TiO_2 or In_2O_3 will be fabricated by the USV team by solution-based methods and subsequently used to fabricate semiconducting films by solution casting and/or spin coating. These films will be interfaced with the dielectric films and metallic electrodes and integrated into FET devices.

2.3. Fabrication and Characterisation of Dielectric Layers by Using Solutions of Colloidal $BaTiO_3$ Nanocrystals

2.3.1 Synthesis, testing and optimisation of properties of dielectric layers containing colloidal $BaTiO_3$ nanoparticles

Thin layers made of close-packed $BaTiO_3$ nanocubes have been fabricated by depositing colloidal solutions containing 15 nm $BaTiO_3$ nanocubes, dispersed in toluene on both rigid (silicon) and flexible substrates (flexible polyamide (Kapton), gelatin, etc.) followed by the controlled evaporation of the solvent. In Figure The surface size of the thin layer represented in Figure 11 is 20 by 20 microns, and the thin layer has a thickness of 300 nm.

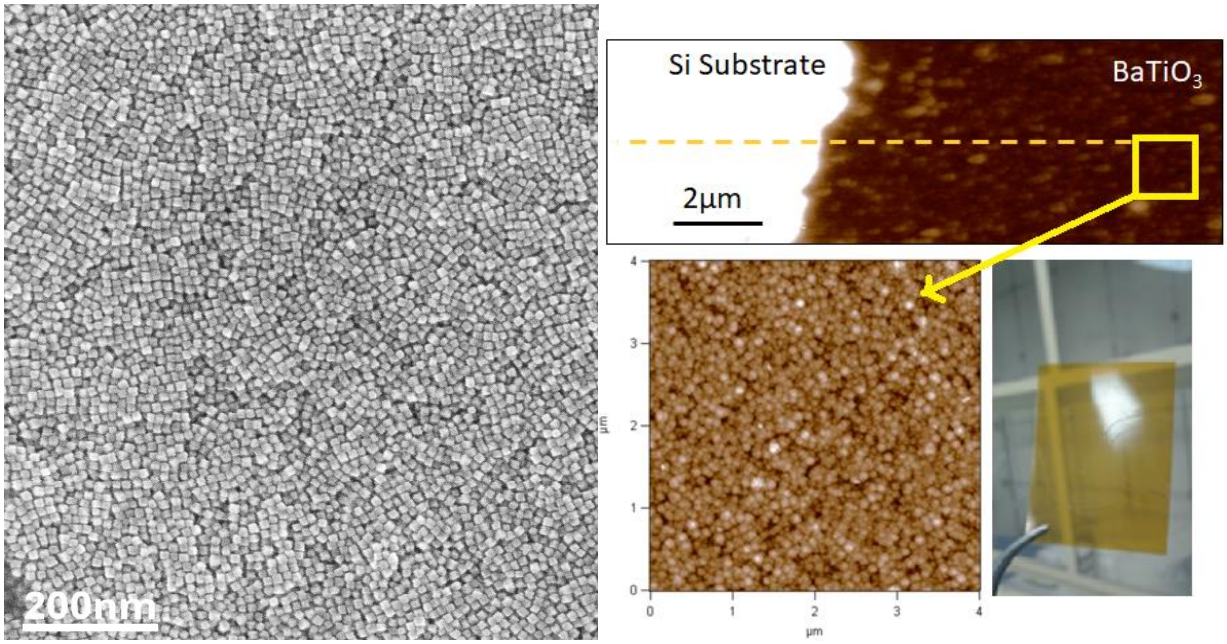

Figure 11. Scanning electron microscopy and AFM images of thin layers deposited on flexible polyimide substrate by direct deposition of colloidal nanoparticle solutions in toluene.

The thickness of the thin layers can be varied in a wide range of values, from tens of nanometers to tens of micrometers by varying both the concentration of nanoparticles in solution, the rate of evaporation of the solvent and the number of deposits made. As can be seen from Figure 10, the thin layers deposited on Kapton foils are transparent, which makes them very attractive for their use in the fabrication of flexible electronic components (planar capacitors or field effect transistors). Figure 12 shows representative scanning electron microscopy (SEM) images of $BaTiO_3$ thin films obtained by deposition from colloidal solutions. The resulting films consist of closely packed nanoparticles and their thickness was varied between 80 nm and 758 nm upon increasing the number of drops of solution cast on the substrate, either rigid or flexible. As a result, the number of deposited layers has increased from 1 to 7. As seen in the plot shown in Figure 12, upon optimizing the concentration of the nanocrystal inks, the thickness a thin layer obtained by casting one individual drop of solution on the substrate was about 100 nm. The thickness of the films and their roughness was routinely investigated by using atomic force microscopy (AFM).

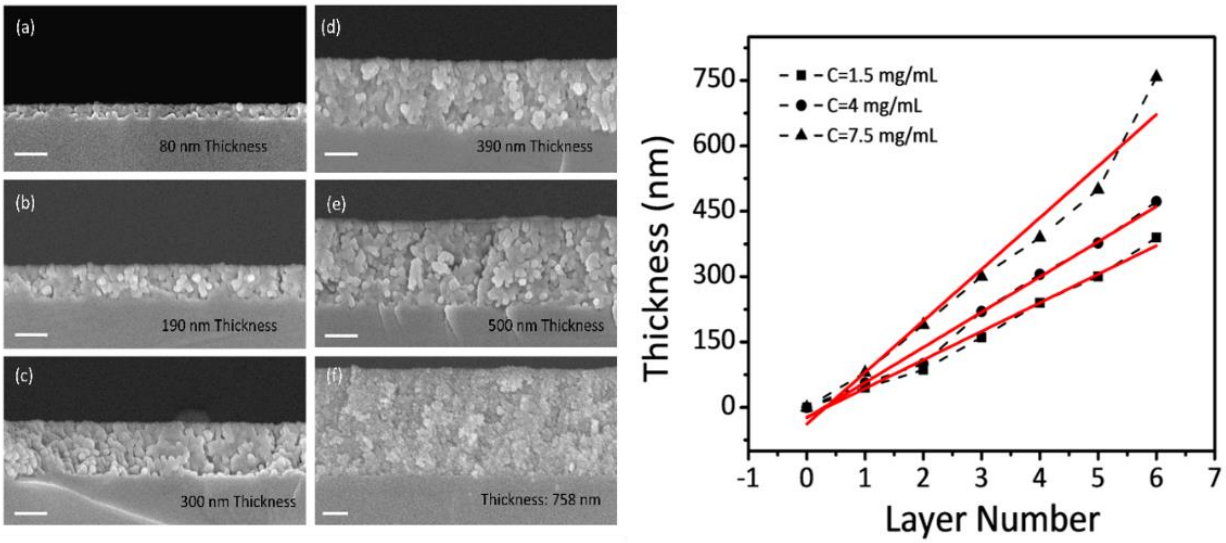

Figure 12. Scanning electron microscopy images of the cross-section of thin layers deposited on flexible polyimide substrate by direct deposition of colloidal solutions of nanoparticles in toluene. The graph on the right illustrates the variation of the thickness of thin layers containing $BaTiO_3$ nanocubes with a size of 15 nm as a function of the number of deposited layers.

In parallel with fabricating nanoparticle-based films by casting colloidal solutions of $BaTiO_3$ nanoparticles, the UAIC team used similar nanopowders which were compacted into pellets and their properties were measured by using different experimental techniques. *The goal of such experiments is two-fold*: *(1) to provide a reference basis for the optimisation of the properties of thin films properties fabricated by using the same type of powders and (2) understand the interplay between the volume and surface/interface contributions to the functional properties of these dielectric materials. The related activities were extended during the first two years.*

To this end, bulk structures (thick films or ceramics) were prepared and investigated (Tasks 1 and 2; Stage 1)) being used as reference systems for the thin films produced from the same type of solutions of colloidal nanoparticles to understand the interplay between the volume and surface/interface contributions to their functional properties. In the frame of activities 1.1.3 and 2.1.3, ***a few types of bulk structures based on $BaTiO_3$ nanoparticles produced by USV and UAIC have been densified by the UAIC*** team using traditional and spark plasma sintering methods. Their dielectric, ferroelectric, tunability, dielectric relaxation – related properties were determined. Since ferroelectric $BaTiO_3$ powders are excellent candidates for the design on magnetoelectric composite materials when interfaced with magnetostrictive phases, such as spinel ferrite oxides MFe_2O_4 (M= first series transition metal) the UAIC team performed some preliminary studies in this direction. Therefore, the UAIC team integrated ferroelectric $BaTiO_3$ thin films along with semiconductor ferrites in magnetoelectric multilayers and performed a comparative study of their properties in contrast with those of randomly mixed phases. Also, preliminary studies aimed at exploring the performance of porous $BaTiO_3$ nanostructures in gas sensing was tested, since the porosity of these dielectric layers makes them good candidates for gas sensing applications. Three main types of thick $BaTiO_3$-structures were studied.

2.3.1.1. $BaTiO_3$-Spinel Ferrite Composites

One of these consisted of $BaTiO_3$-ferrite composites, whereby the ferrite phase was either pure or Zn-doped $CoFe_2O_4$ (CF) to perform a comparative study on the impact of the phase arrangement; that is random mixing (3-3) *vs.* layered structures (2-2) on the structural, microstructural and functional properties. The use of fast consolidation (SPS) and optimized processing parameters provided pure di-phase composites with limited interphase reactions, as shown by structure refinements by the Rietveld method (Figure 13).

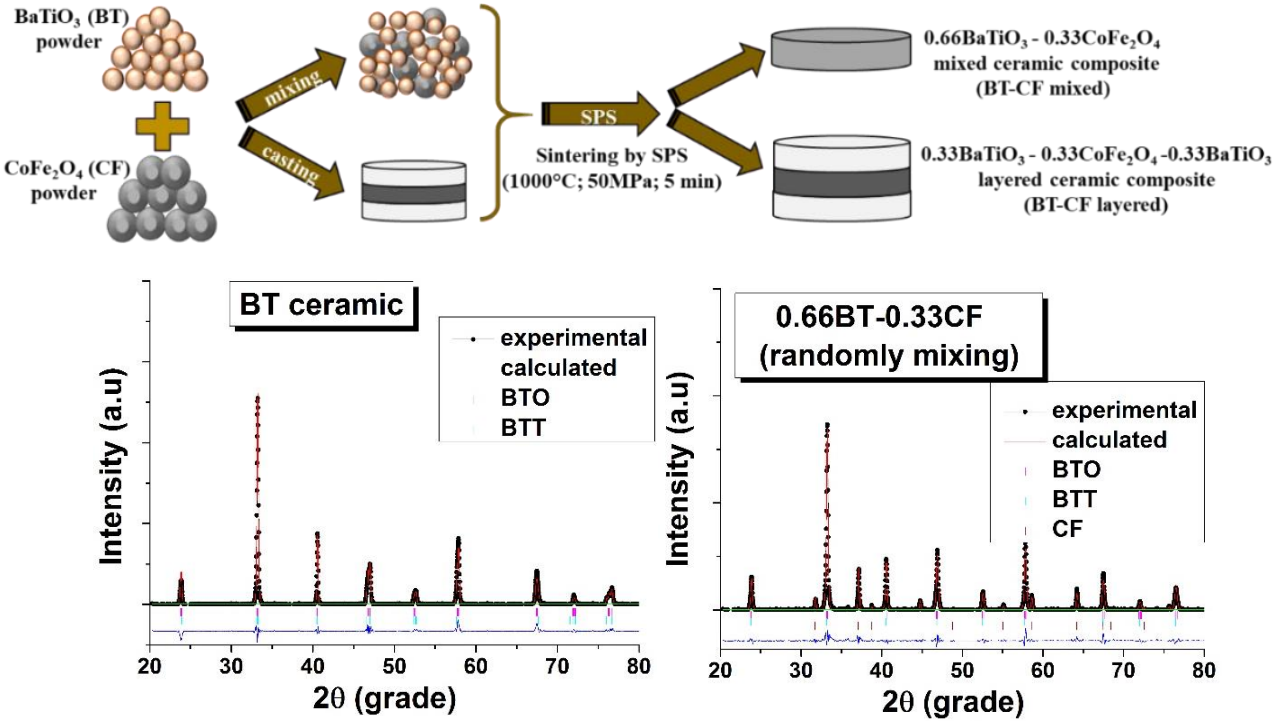

Figure 13. Schematic representation of the procedure used to fabricate magnetoelectric composites contaoning BaTiO3 and a ferrite phase (top images) and structure refinement plots of the BT phase and randomly mixed $0.66BaTiO_3$–$0.33CoFe_2O_4$ composite by using the Rietveld method (bottom images).

The linear and non-linear dielectric properties investigated by using a broad spectrum of frequency and temperature range indicated a higher dielectric permittivity and lower loss for the (3-3) configuration. However, such a geometry of the magnetoelectric composite showed limitations in performance, specifically a lower dc conductivity in the range of (10^{-11} -10^{-5}) S/cm compared to vales ranging from 10^{-12} to 10^{-7} S/cm observed for the (2-2) structure. Regardless of the type of connectivity between phases in the magnetoelectric composite material (2-2 or 3-3) the ferroelectric P(E) loops were found to be affected by the resistivity loss. The loss mechanisms were described comparatively: a thermally activated loss mechanism with a 0.5 eV activation energy was typical for both configurations. However, the (3-3) magnetoelectric composite material was found to also exhibit a conductivity dispersion mechanism with a lower activation energy of 0.3 eV (Figure 14). These findings suggest that the magnetoelectric nanocomposites made from compacted $BaTiO_3$ (BTO) powders in combination with a spinel ferrite and 2-2 or 3-3 connectivity schemes could be potentially attractive to various applications. *The results of this*

collaborative effort between the USV and UAIC teams were published (grant members underlined) in a Q1 journal (A. Guzu, C.E. Ciomaga, M. Airimioaei, L. Padurariu, L.P. Curecheriu, I. Dumitru, F. Gheorghiu, G. Stoian, M. Grigoras, N. Lupu, M. Asandulesa, L. Mitoseriu, Functional properties of randomly mixed and layered $BaTiO_3$-$CoFe_2O_4$ ceramic composites close to the percolation limit, J. Alloys & Compounds **2019**, 796, 55-64 (2019).

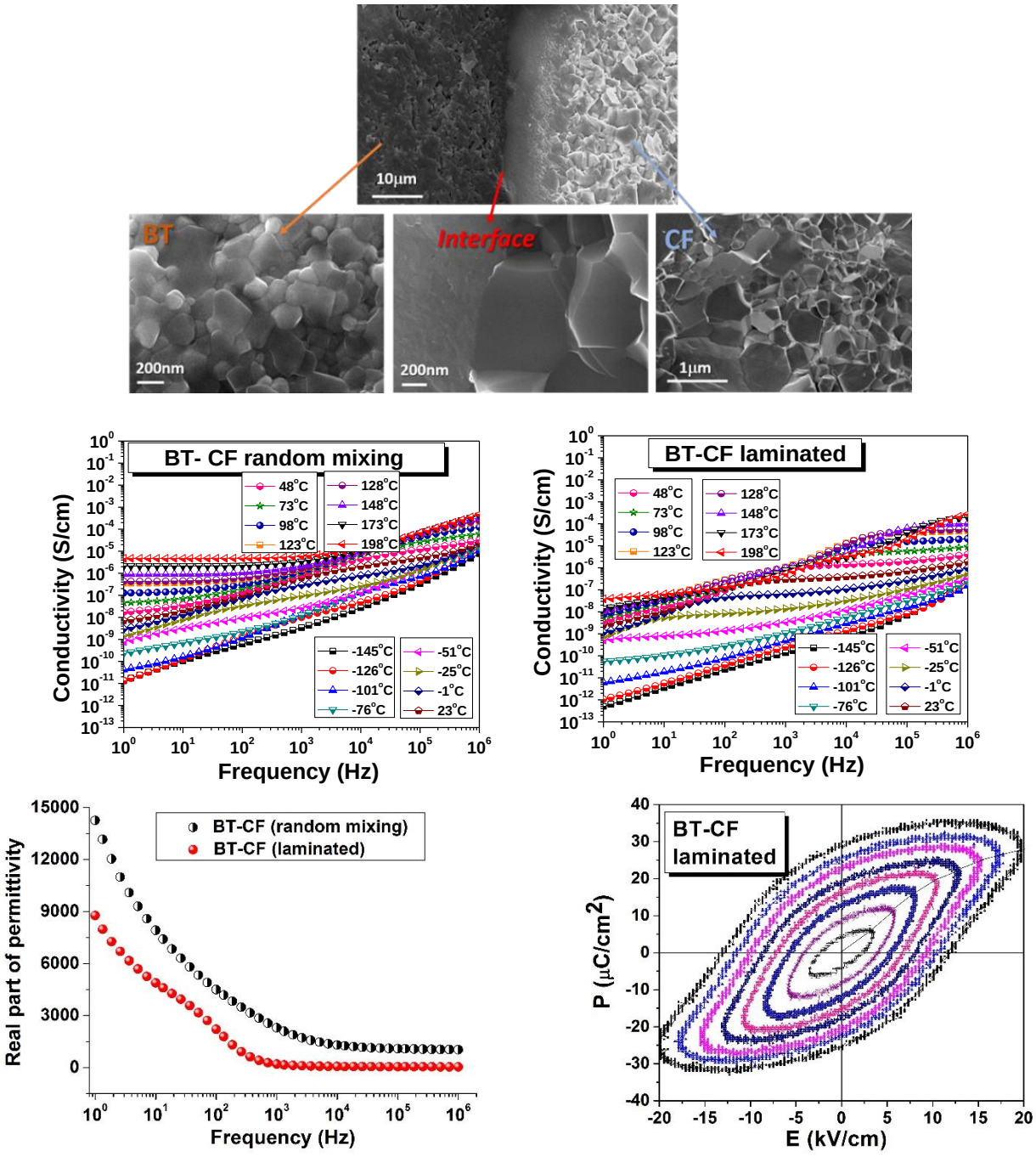

Figure 14. Micrographs of the interface between BTO and CF layers, comparative conductivity, permittivity *vs.* frequency and P(E) loops in BTO-CF layered and mixed structures.

Furthermore, $BaTiO_3$-$Co_{0.8}Zn_{0.2}Fe_2O_4$ (BT-CZF) layered and mixed ceramics were produced and their properties investigated. The role of the processing parameters (the type and parameters used in the sintering

process) on the microstructure (grain size, density and small doping level at interfaces) was studied, while keeping the same type of connectivity scheme (3-3). At 500 kHz, the permittivity ranges between ε=360 and ε=900 for the composite sintered by the traditional method and between ε=200 and ε=400, with an excellent thermal stability for the composite sintered by SPS in a broad temperature range (t=-150, 200)°C. (Figure 15).

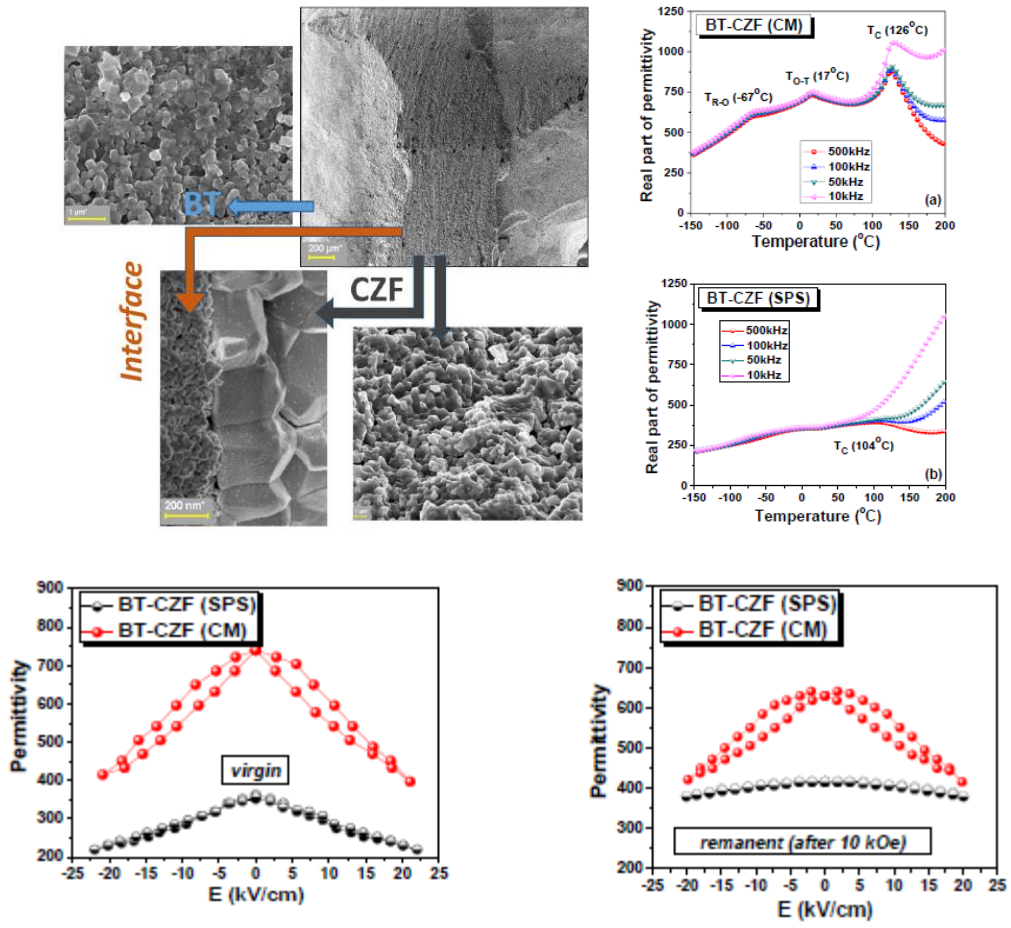

Figure 15. Micrographs showing the ceramic grains and interfaces between BT and CZF layers and influence of grain size on the permittivity *vs*. temperature dependences. Bi-tunable character of permittivity is illustrated by ε(E) dependences at H=0 (virgin) and after the application of a magnetic field H=10 kOe (remanent).

These differences between the dielectric properties of composites with the same composition and connectivity schemes but obtained by two different processing methods were ascribed to micro/nanostructural differences; that is ultrafine grains in the ceramic composite processed by the SPS technique. A very interesting feature is that the magnetoelectric composites *show a bi-tunable character, i.e. a variation of permittivity under both an electric and a magnetic field (Figure 15).* The composites tested in a microwave resonator demonstrated a shift of the resonance magnetic mode $TEme_{010}$ upon the application of a magnetic field H=1.9 kOe (10 times higher than the coercive magnetic field), due to the existence of an indirect magnetoelectric coupling. This property makes these composites very interesting for applications in microwave filters. *The results were published (grant members underlined) in a Q1 journal: C.E. Ciomaga, A. Guzu, M. Airimioaei, L.P. Curecheriu, V.A. Lukacs, O.G. Avadanei, G. Stoian,*

M. Grigoras, N. Lupu, M. Asandulesa, L. Mitoseriu, Comparative study of magnetoelectric $BaTiO_3$–$Co_{0.8}Zn_{0.2}Fe_2O_4$ bi-tunable ceramics sintered by Spark Plasma Sintering and classical method, Ceram. Int. **2019**, *45*, 24168-24175.

2.3.1.2 Self-organised $Ba_{12}Fe_{28}Ti_{15}O_{84}$ layered structures obtained from $BaTiO_3$ - Fe_2O_3 nanocomposites.

A detailed structural analysis indicated the formation of monoclinic space group *C*2/*m* (278 ions - 2 chemical formula units/unit cell and lattice parameters: *a* = 9.988(1) Å, *b* = 17.298(2) Å, *c* = 19.17(4) Å and β = 99.33°), with an intergrowth of BT perovskite-like and ferrite spinel-like blocks, with the Ti^{4+} ions in octahedral coordination into the perovskite-like structural units and Fe^{3+} ions, predominantly occupying tetrahedral sites, into spinel-like layers. Due to its complex structure, it is *a smart multifunctional material*, exhibiting at least *four types of functional properties at room temperature*. Specifically, it is thermoelectric with a prominent thermopower and low thermal conductivity, has a nonlinear dielectric character (significant tunability) and is a multiferroic (*i.e.* possesses both ferroelectric and magnetic order) (Figure 16). Also, it exhibits semiconductor properties with thermally activated ac/dc conductivity and multiple dielectric relaxations due to Maxwell-Wagner contributions and shows a strong magnetic response both at nanoscale and at macroscopic level. *The layered structure is a natural self-assembled material which is interesting as an optimised model system with perfect assembly for the tasks concerning $BaTiO_3$-based integrated thin films with expected multi-functional character*.

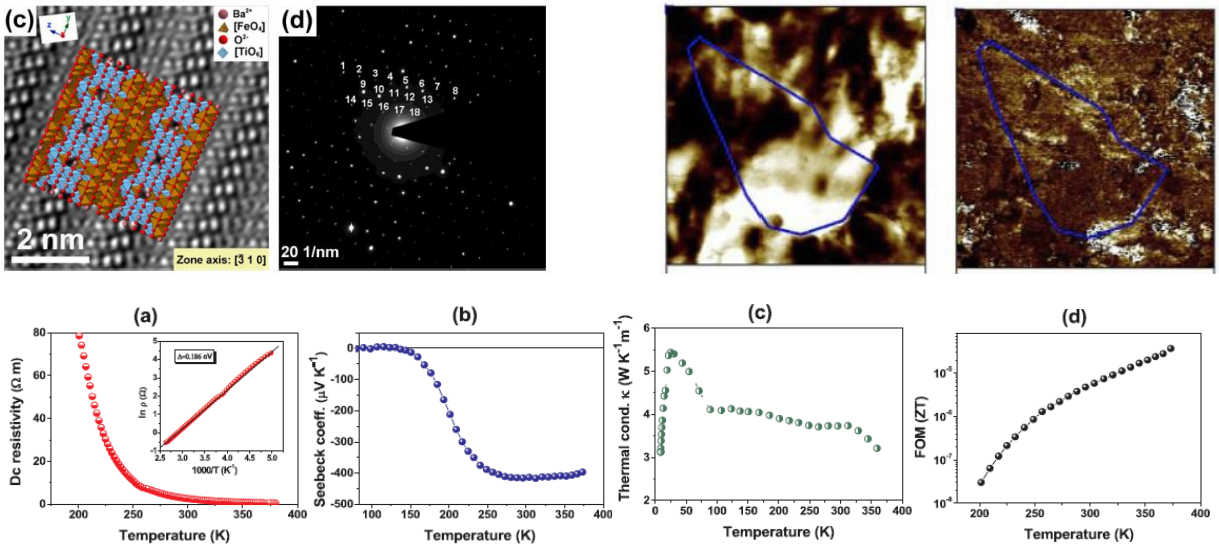

Figure 16. HRTEM analysis showing the nanoscale layered arrangement, PFM and MFM local response and macroscopic functional properties *vs.* temperature of $Ba_{12}Fe_{28}Ti_{15}O_{84}$ system.

The results were published in an internationally collaborative scientific paper (grant members underlined) in a Q1 journal: L. Curecheriu, C. Harnagea, M.T. Buscaglia, I. Pallecchi, B.S. Vasile, V.A. Surdu, A.C. Ianculescu, A. Pignolet, F. Rosei, L. Mitoseriu, V. Buscaglia, Four-fold multifunctional properties in self-organized layered ferrite, Ceram. Int. **2020**, *46*, 28621–28630.

2.3.1.3. $BaTiO_3$ Nanocubes as Building blocks for porous structures with conserved microstructures

$BaTiO_3$ nanopowders with cube-like morphology, with a sharp lognormal particle size distribution ranging between 5–25 nm and average size of 16 nm produced by USV were employed by UAIC group to produce by partial sintering nanostructured ceramics with high porosity level around the percolation limit (33%, 37% relative porosity) by field-assisted fast sintering. By finding appropriate sintering parameters, not only *a high porosity* was be reached together with a *good mechanically stability*, but also the *morphology of starting cubic-like nanopowders was preserved* into the consolidated product, which represents **a novel result at international level** *(Figure 17*).

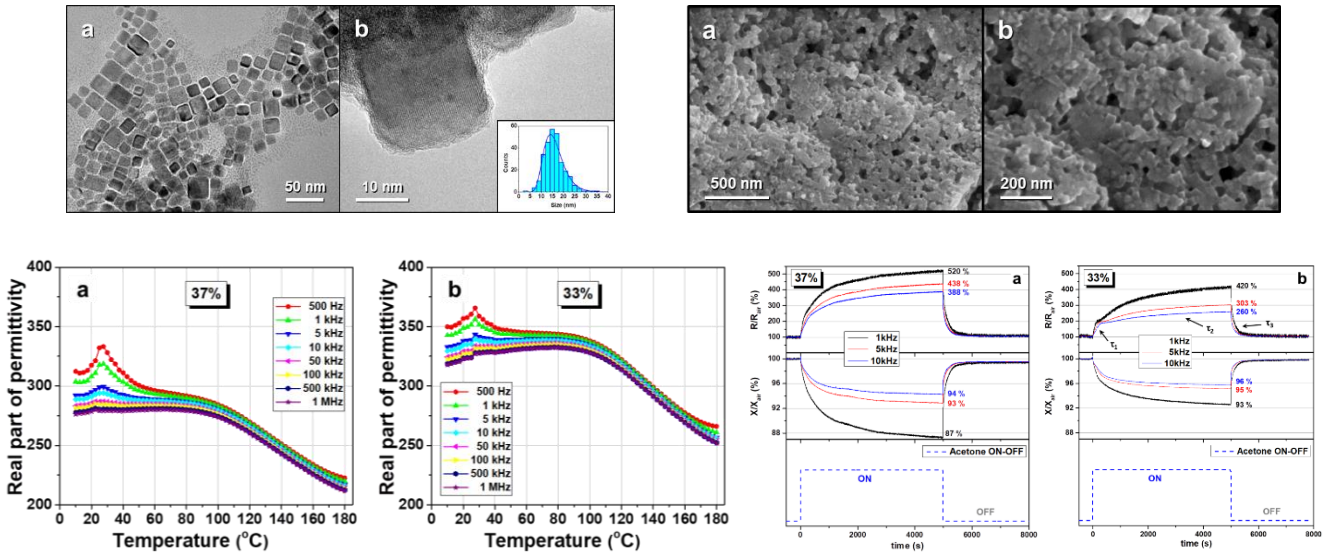

Figure 17. Cubic $BaTiO_3$ nanopowders, porous ceramics with preserved cube-like grains and their dielectric and gas sensitivity response.

Most experimental methods used to compact dielectric nanograins into dense ceramics are limited to materials in which the constituents lose their individual morphology. Our teams mitigated this problem for the first time by a fast sintering with SPS technique and the results obtained are very promising. The potential of SPS technique was just recently recognised for producing porous materials (D. V. Dudina *et al.*, *Fabrication of porous materials by spark plasma sintering: A Review, Materials* (Basel) **2019**, (12), 541). The resulted ceramics have cuboid shape grains of 10-40 nm range, with regions of self-assembled cubic grain arrangements and *multiscale porosity level ranging from a few nm cubic pores to hundreds nm.* The dielectric response is dominated around room temperature by a prominent interface-driven Maxwell-Wagner conductivity relaxation, which is related to the gas and water molecule adsorption at the porous ceramic interfaces. This feature indicated a potential high room temperature sensitivity of the electrical properties to interface-driven phenomena, *e.g.* gas adsorption at ceramic-pore interfaces. This hypothesis was checked by performing preliminary gas sensing tests in dynamic regime, at normal room temperature and pressure conditions, using acetone as testing gas. Porous $BaTiO_3$ ceramics with cubic-like grains show a high level of replicability under repeated cycles of testing and higher sensitivity at lower frequency, in

both real and imaginary part of their impedances. *The results were published (grant members underlined) in a Q1 journal: V.A. Lukacs, G. Caruntu, O. Condurache, C.E. Ciomaga, L.P. Curecheriu, L. Padurariu, M. Ignat, M. Airimioaei, G. Stoian, A. Rotaru, L. Mitoseriu, Preparation and properties of porous $BaTiO_3$ nanostructured ceramics produced from cuboidal nanocrystals, Ceram. Int., available online (2021): https://doi.org/10.1016/j.ceramint.2021.03.128*

It is worth mentioning that regardless of their chemical composition nanoparticle-based films are notoriously porous, the presence of air voids being detrimental to the value of their dielectric constant. Therefore, the study of porous bulk ceramics with cubic grains is important as a reference for comparing their properties with ones obtained in close-packed thin films in the view of their integration. This approach is key in understanding the interplay between the volume/surface and interface effects on the electrical properties of ferroelectric nanoparticle-based thin films.

2.4. Fabrication of Flexible Polymer-Ceramic Composites Based on $BaTiO_3$ Nanocrystals

In the first two years of the project, the research activities of the USV and UAIC teams related to Task 2 were focused to the design of novel polymer-ceramic nanocomposite films by using different types of polymers, whereas the NIMP partner was involved in the structural characterization of such composite materials. The rationale used to select the polymers was their polar/non-polar character, which should be like that of the dielectric/ferroelectric nanocrystals, their solution processability and relative higher value of their dielectric constant. Such composites started to be incorporated into flexible capacitors and FETs during Year 2. The best composite structures in terms of filler homogeneity, lack of agglomeration into the polymeric matrix, flexibility, smooth surfaces, reduced porosity, increased permittivity, and low dielectric losses will be used in Years 3 and 4 to fabricate flexible capacitors and FET prototypes, whose electrical performance will be tested and continuously optimized.

Polymer–ceramic nanocomposite films consisting of ceramic nanoparticles dispersed into a polymer matrix (0–3 composites) have garnered increasing interest due to their superior performance characteristics, which can be used in flexible modern electronics and energy storage systems. Our first work reports on the rational design of substrate-free polymer ceramic nanocomposite films consisting of differently sized (10 nm and 20 nm), oleic acid-coated $BaTiO_3$ colloidal nanocrystals dispersed into styrene butadiene styrene (SBS) by using a highly reliable solution-based method. The amount of filler nanoparticles was varied from 0 to 50 wt.% and the resulting films preserved their original mechanical properties, without signs of brittleness or defects. The effect of the size and weight fraction of the filler nanoparticles on the morphology and the dielectric properties of the BTO–SBS nanocomposite films was systematically investigated. Electron microscopy images showed that the filler nanoparticles are uniformly distributed within the SBS matrix with a substantial decrease of the interparticle distance within the elastomer matrix when the filler content was varied from 10 to 50 wt.% (Figure 18).

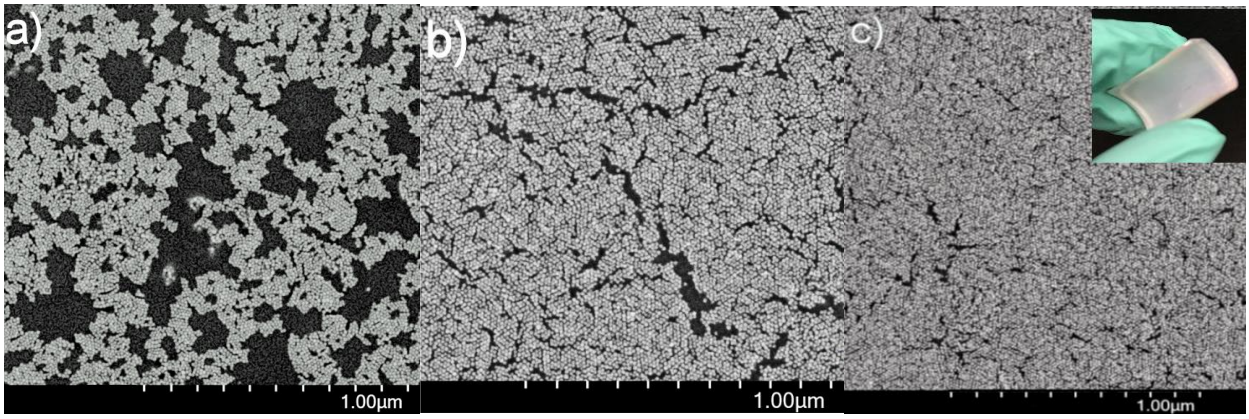

Figure 18. Surface field emission scanning electron microscopy micrographs of BaTiO–SBS nanocomposite films with a content of 30% (a); 40% (b) and 50% (c) 10 nm BaTiO3 colloidal nanocrystals as ceramic fillers.

The morphology and surface topology of the BTO-SBS nanocomposite films obtained by incorporating 10 nm $BaTiO_3$ nanocubes into the elastomer matrix have been investigated by atomic force microscopy (AFM), the corresponding images being presented in Figure 19. The images clearly show that the nanocomposite films are uniform and possess a roughness that changed from 3.0 nm for the neat SBS polymer to 32.5 nm for the (50 % wt.) BTO-SBS nanocomposite film for a raster scanned area of 5 μm^2.

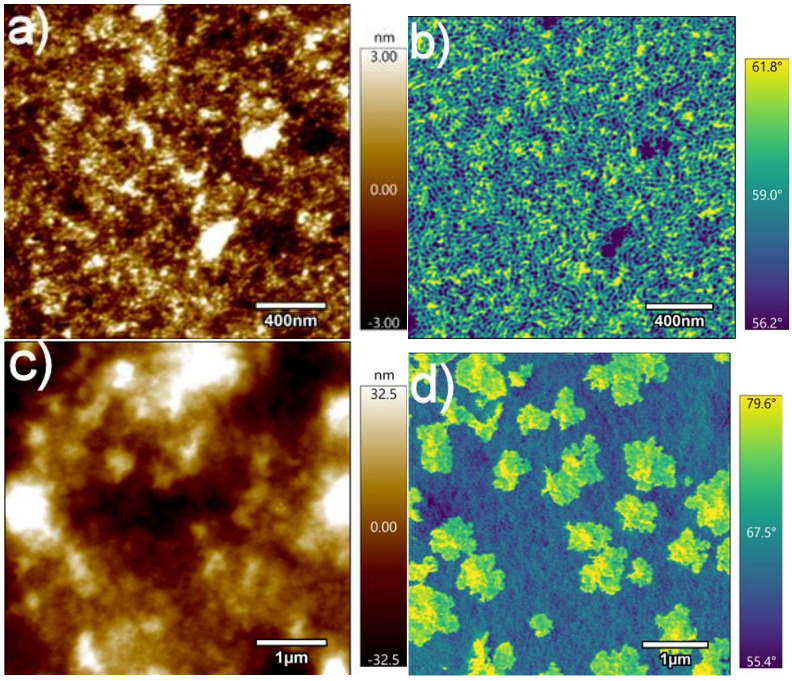

Figure 19. Atomic force microscopy images of the neat SBS film (a) and a (50% wt.) BTO-SBS nanocomposite film.

Room temperature dielectric spectroscopy data (Figure 20) showed that the dielectric constant of the SBS elastomer improved significantly (from ε=4 to ε=34.3 and ε=33.7 upon incorporating 10 nm and 20 nm $BaTiO_3$ nanocubes). The breakdown field values were found to decrease from 195 kV/cm^{-1} for the neat elastomer to 15 kV cm−1 for the SBS–BTO nanocomposite films with 50% (wt.) filler nanoparticles. As shown in Figures 9a and 9c, the real part of the dielectric constant of BTO-SBS nanocomposite film containing 10 nm and 20 nm $BaTiO_3$ nanocubes dispersed into the elastomer matrix with concentrations of the filler nanoparticles in the range from 10 to 50 % showed a weak dielectric dispersion in the whole frequency range (from 100 Hz to 1 MHz) which makes these nanocomposite materials attractive for high frequency applications. Specifically, the dielectric constant of BTO-SBS nanocomposite films containing 10 nm $BaTiO_3$ nanocubes with a filler concentration ranging from 10 to 50 wt. % was found to decrease by 3.13 % and 6.69 % in the frequency range from 100 Hz to 1

MHz, whereas for 20 nm nanocubes this decrease was by 1.42 % and 7.11 % for the same filler concentration and frequency range, respectively. The decrease of the dielectric constant values with the frequency has been ascribed to the dielectric relaxation of the $BaTiO_3$ nanoparticles and the existence of interfaces due to the uniform dispersion of the filler nanocrystals within the elastomer matrix. Also, at high frequencies, there is a lag time between the field reversal and the reorientation of the dipoles, which leads to a decrease of the value of the dielectric constant due to the relaxation of electrical dipoles.

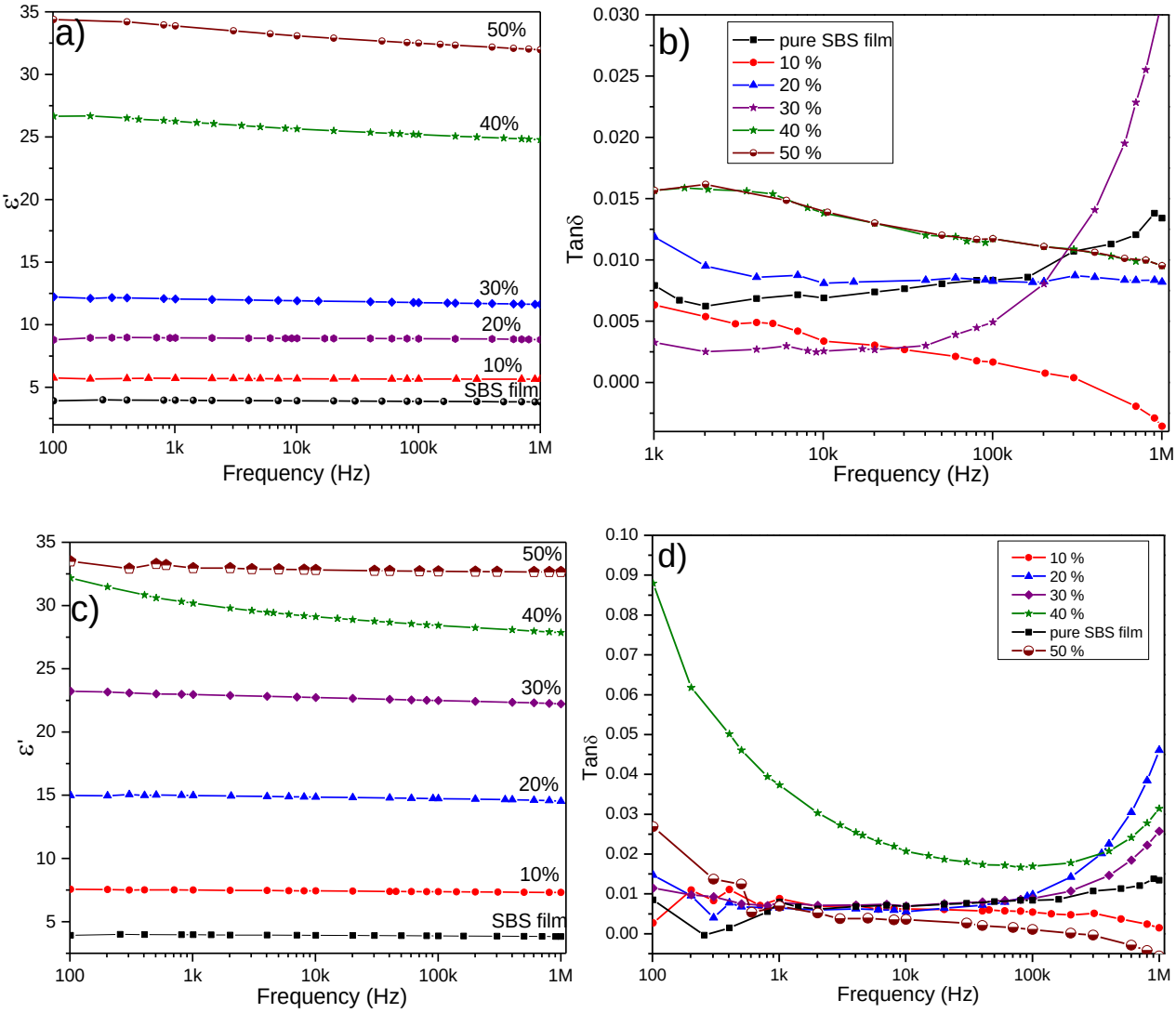

Figure 20. Frequency dependence of the relative dielectric constant (ε') and loss tangent of BTO–SBS nanocomposite films made by using 10 nm (Fig. 19a and b) and 20 nm (Fig. 19c and d) $BaTiO_3$ nanocubes. The concentration of the filler nanoparticles ranged between 0 and 40 wt. %, respectively.

The experimental results show that these BTO–SBS nanocomposite thin films exhibit superior properties, which make them attractive for implementation in high-performance capacitive storage devices, wearable technology, sensors and nanoelectronics. We show that the BTO–SBS nanocomposite films fabricated by the proposed approach present high permittivity values along with excellent mechanical properties and can be potentially used in energy storage applications. *The results were published (grant members underlined) in a Q1 journal: D. Caruntu, B. Kavey, S. Paul, A.C. Bas, A. Rotaru, G. Caruntu, "Dielectric properties of*

solution-processed $BaTiO_3$–styrene butadiene styrene nanocomposite films", CrystEngComm, **2020**, *22 1261-1272.*

Starting the second year, a few types of flexible composites based on $BaTiO_3$ nanocube-like fillers (with an average particle size of 15 nm) produced by USV and characterized from microstructural point of view by NIMP were embedded in polymer matrices as PVDF, epoxy resin or gelatin biopolymer by solution casting. Their electrical properties have been compared with similar composites in which spherical BT particles with the same average particle size were used as filler, in order to observe if the cubic-like shape plays any role on the electrical properties (related to possible electric field enhancement in sharp regions). The structural, microstructural, dielectric, ferroelectric and piezoelectric properties of such composites have been investigated by UAIC. As a matrix, three types of polymers have been tested: (i) epoxy resin, (ii) polyvinylidene fluoride – PVDF and (iv) gelatin bio-polymer, respectively.

(i) The preliminary study on epoxy-BT composites show an increase of permittivity when increasing the addition of BT (almost twice higher in 5%BT with respect of one of epoxy matrix) and show room temperature losses below 6% in overal the investigated radiofrequency range. The *ac* conductivity linearly increased in log-log scale for frequencies above 100 Hz and does not show any significant relaxations. The ac resistivity ranges between $3x10^9$ Ω/m and 10^{11} Ω/m. However, for high BTO contents the porosity was not controlled, and permittivity becomes even lower than in pure epoxy (Figure 21), this indicating that the homogenization of these composites should be further optimized and solvent evaporation during co-polymerization of epoxy bicomponent should be better controlled in the next steps.

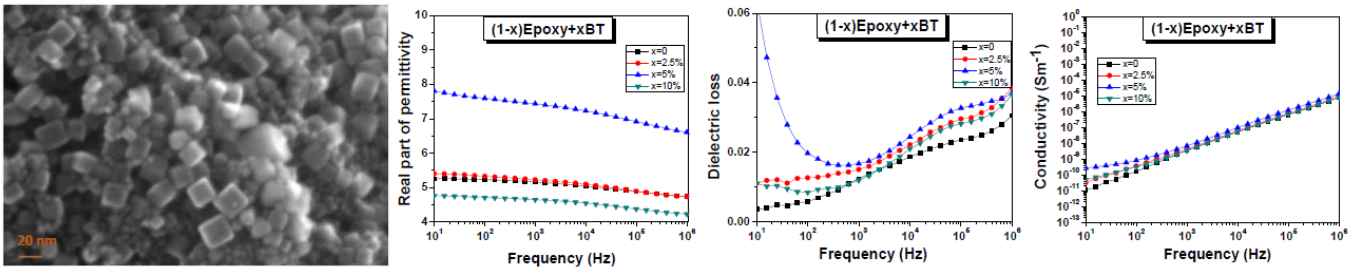

Figure 21. SEM micrographs of starting BT nanocubes used for preparing polymer-based composites; permittivity, dielectric loss and ac conductivity vs. frequency for BT-epoxy composites.

(ii) The attempts to prepare composites by using BT nanocubes, BT spherical nanoparticles or other nanoparticles within PVDF ferroelectric matrix have shown *limitations of solution-based methods in eliminating porosity* in this type of materials and optimization of preparation have to be further realized when using PVDF. Better density was realized by a collaboration between UAIC and NIMP in producing flexible PVDF films by using larger particles (*e.g.*, micron $Ba_{12}Fe_{28}Ti_{15}O_{84}$), which can be better isolated and dispersed within the polymer matrix and better densification was achieved. The composites remained flexible until max. 9 wt.% filler addition and have shown a multifunctional character: dual magneto-piezoelectric response with reasonable dielectric, ferro/piezoelectric and soft magnetic character, while

maintaining a high flexibility. *These results were published in a Q2 journal (grant members underlined): F. Gheorghiu, R. Stanculescu, L. Curecheriu, E. Brunengo, P. Stagnaro, V. Tiron, P. Postolache, M.T. Buscaglia, L. Mitoseriu, PVDF–ferrite composites with dual magneto-piezoelectric response for flexible electronics applications: synthesis and functional properties, J. Mater. Sci. 55, 3926–3939 (2020)*

An alternate way to remove porosity in PVDF-BT nanocomposites was also explored by an external collaboration by using a solvent-free method, *i.e.* by hot-molding (which is a technique not available in our group of partners). By this method, successful densification to 100% of BT-PVDF composites could be realized and this study resulted in a publication, in which UAIC contribution was to realise the full electrical characterisation of such PVDF-BT composites. *These results were published in a Q2 journal (grant members underlined): E. Brunengo, L. Conzatti, I. Schizzi, M.T. Buscaglia, G. Canu, L. Curecheriu, C. Costa, M. Castellano, L. Mitoseriu, P. Stagnaro, V. Buscaglia, Improved dielectric properties of poly(vinylidene fluoride)-$BaTiO_3$ composites by solvent-free processing, J. Appl. Polym. Sci. 138, 12, 50049 (2021)*

(iii) Promising results in terms of processing flexible composites (*i.e.* a better densification, homogeneous distribution of filler) were realized by UAIC using gelatin biopolymer as matrix with optimized BT nanocube fillers produced by USV. Gelatin is a natural protein-based compound derived by partial hydrolysis of native collagen existing in skin, tendons and bones of animals and is a very interesting material as matrix for non-toxic "green electronics" (bio-degradable, recyclable and bio-compatible). Gelatin is a polar polymer showing electroactive properties and has potential in integrated optical and electrical devices. By using a solvent-based method, flexible thick films xBTO-(1-x)gel with compositions x=0, 6.25, 18, 25 and 40 wt. % were obtained (Figure 22) with a rather homogeneous dispersion of BT nanocubes within the matrix volume. The room temperature dielectric characterisation in the frequency range ν=1-10^6 Hz indicated a slight increase of permittivity due to the BT nanoparticles addition from 9 (x=0) to 15 (x=40%) at 10^5Hz (Figure 22) and low dielectric losses ~3-5%,

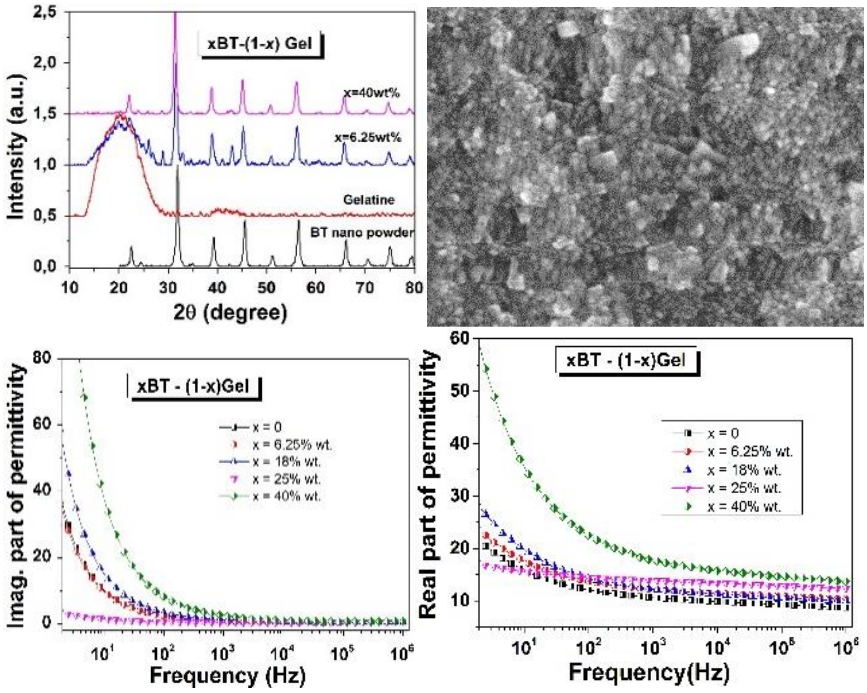

Figure. 22. XRD patterns of xBT-(1-x)Gel thick films and microstructure for x=40% wt. Room temperature dielectric characteristics *vs.* frequency for xBT-(1-*x*)Gel (*x*=0, 6.25, 18, 25 and 40.

indicating a good dielectric character. Strong Maxwell-Wagner relaxations due to space charge effect at multiple BT-polymer interfaces are found below 100Hz in all the composites and mostly for ones with high BT additions, for which permittivity reaches at 10Hz high values of 50-60 (x=40%) with respect to 20 (x=0), but they are also accompanied by high resistive losses.

2.5. Contributions to Activities 3.3.4 (3. Integration of thin dielectric layers in flexible capacitors and optimisation of their performances)

Further, the room temperature polarisation *vs.* field dependences P(E) have been determined at different frequencies and the results for f=100 Hz are comparatively shown in Figure 23.

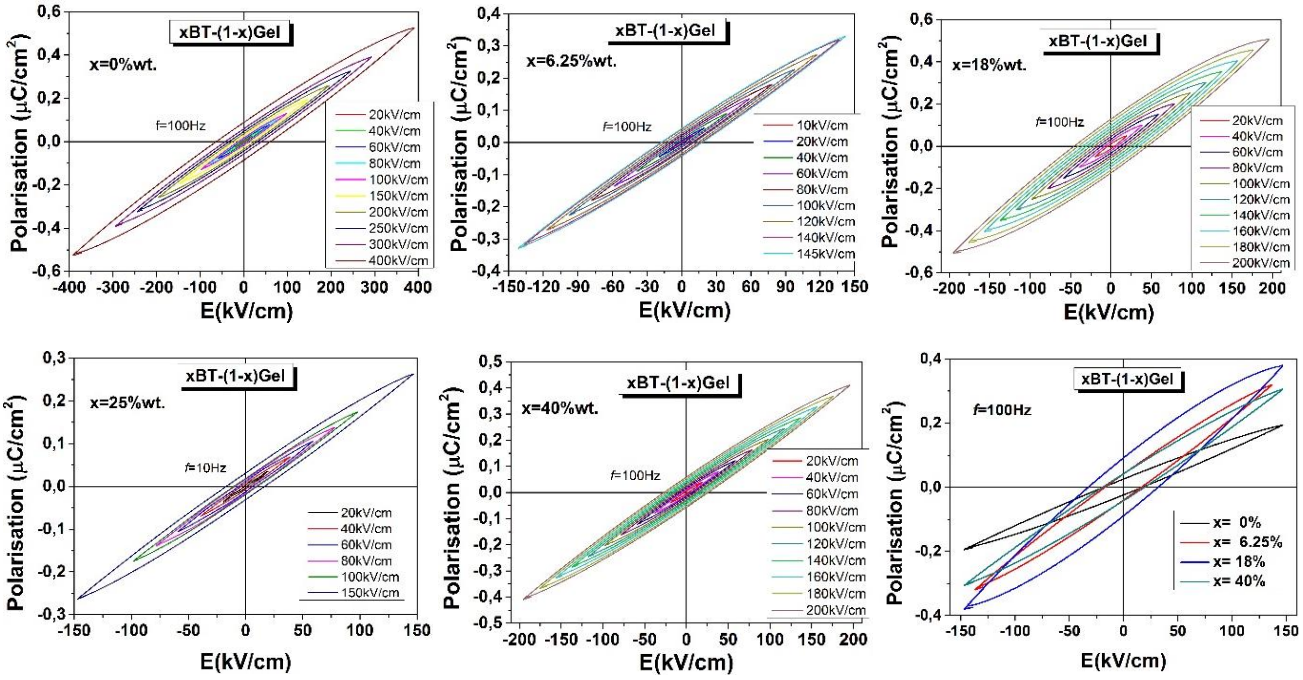

Figure 23. P(E) minor loops at f=100 Hz for xBT-(1-*x*)Gel flexible composite films (*x*=0, 6.25, 18, 25 and 40%)

Together with the dielectric permittivity, polarisation increases with the addition of BT nanoparticles, but in the range of fields below the breakdown, a linear dielectric character was only observed (equivalent with an RC group). The recovered energy density (W_{rec}) and stored energy density (W_{stored}) in the volume unit were determined from the *P(E)* loops (Figure 24) for fields in the range ($-E_{max}$, + E_{max}) by using the formulas:

$$W_{rec} = \int_{P_r}^{P_{max}} EdP \qquad W_{stored} = \int_{P_{-r}}^{P_{max}} EdP$$

and the energy storing efficiency is: $\eta = \frac{W_{rec}}{W_{stored}}\ x\ 100\%$, where: $W_{stored} = W_{rec} + W_{loss}$.

Among this series of flexible composites, x=18% shows the highest stored energy density of 36 mJ/cm^3, but its efficiency is 50%, while the highest efficiency of 70% is found for x=6.25% with a stored energy density of 25.3 mJ/cm^3. The values are very low with respect to the best ones reported in literature for

similar composites [S. Luo *et al., Adv. Energy Mater*. **2018**, *9(5)*, 1803204], but they are still promising by considering the low level of the applied maximum field.

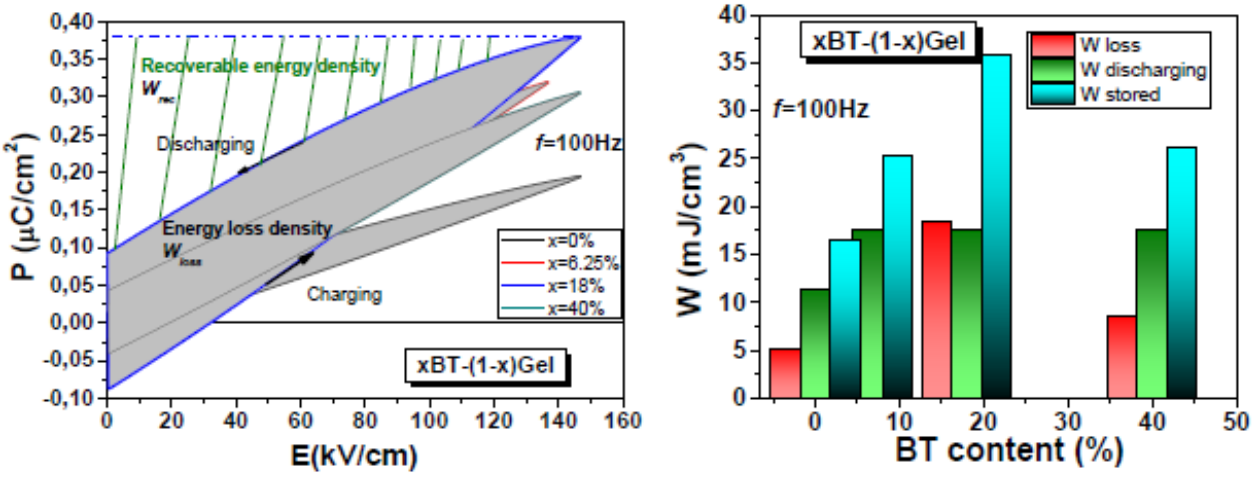

Figure 24. P(E) loops; loss, discharging and stored energy density for xBT-(1-x)gel.

The attempts to produce an increase of permittivity in flexible polymer-based composites by using BT nanocubes and various polymers as matrices resulted in a modest permittivity rise (about 2-3 times) with respect to ones of the pure polymers, due to several factors:

- Inherent porosity in composites processed by solution casting. Porosity is detrimental because it reduces the permittivity enhancement realised by the presence of filler, but also because limits the maximum applied voltage by reducing the breakdown field. Increasing the filler composition above 40% would strongly reduce the composites flexibility. Optimisation of processing parameters still has to continue in the next year for enhancing energy storage ability;
- Ultrafine BT nanoparticles have a very small permittivity and polarisation with respect to their micron-sized counterparts, as result of scale-dependent properties decay. Cube-like particles with larger grain size should be further employed to increase more the composites permittivity. However, coarse grained particles limit the solution-based processability of such composites and their flexibility; a compromise for optimum properties should be found;
- A possible solution to maintain flexibility and increase even more the permittivity in composites is to embed ultrafine metallic nanoparticles besides BT nanocubes as fillers. This emergent route will be explored in the next years.

2.6. Contributions to the activities 3.1.2 (3. Integration of thin dielectric layers in flexible capacitors and optimisation of their performances)

Modeling: In paralel with the experimental work aimed at the fabrication of polymer-based BT nanocomposites, we developed a theoretical modeling-based estimation of the influence of fillers with higher permittivity into a low permittivity polymer matrix on the the dielectric properties of the nanocomposite. To this end, simulations were performed by using Finite Element Methods (FEM) applied

to composites formed by a low-permittivity polymer matrix with ferroelectric nanoparticles as fillers (e.g. $BaTiO_3$). In the first step, the influence of the filler particles shape on the dielectric properties of composites for the same concentration was investigated. Numerical mehods developed by UAIC and experimentally validated for the case of other inhomogeneous dielectrics or composites were employed. The FEM codes solve the Laplace equation: $(\nabla \cdot (\varepsilon \nabla V) = 0$, where ε is the relative permittivity and V is the local potential under the border condition of plan-parallel capacitance. It was developed a procedure to generate random 3D microstructures similar as provided from experimental SEM micrographs for the BT-polymer composites, in which two types of filler geometries were compared: cubic (Figure 25) and spherical (Figure 26).

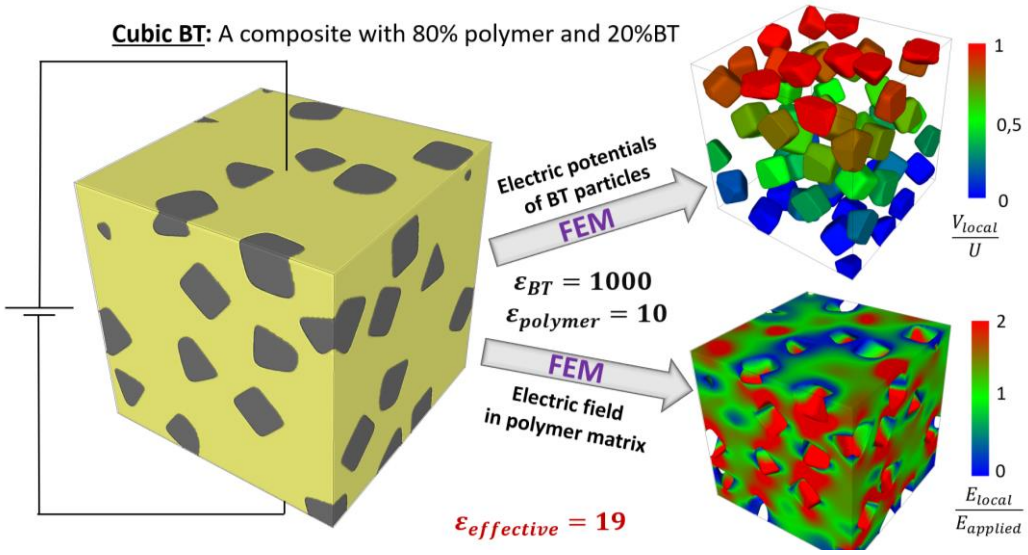

Figure 25. Simulation of local potential and fields and estimation of effective permittivity for a composite with 20% cubic BT nanoparticles within a polymer matrix.

The random cubic fillers were generated by the following procedure:

- Randomly generating of cube centres with coordinates: x_{ci}, y_{ci} și y_{ci}, where *i* is the cube index;
- Randomly generation of axes orientations by versors $\overrightarrow{u_{xi}}$, $\overrightarrow{u_{yi}}$ și $\overrightarrow{u_{zi}}$;
- Building the cubes according to the equation: $\left(\frac{x^*}{10nm}\right)^6 + \left(\frac{y^*}{10nm}\right)^6 + \left(\frac{z^*}{10nm}\right)^6 = 1$, where x^*, y^* and z^* are the coordinates on the cube surface in the local coordinate system defined by the resors generated at the previous step.

The random spheric fillers were generated by the following procedure:

- Randomly generating of sphere centres with coordinates: x_{ci}, y_{ci} și y_{ci}, where *i* is the sphere index;
- Building the spheres according to the eq.: $\left(\frac{x-x_{ci}}{10nm}\right)^2 + \left(\frac{y-y_{ci}}{10nm}\right)^2 + \left(\frac{z-z_{ci}}{10nm}\right)^2 = 1$, where *x* , *y* and *z* are the coordinates of points on the i^{th} sphere surfaces in the capacitor coordinate system (i.e. Oz is the field direction, perpendicular on the electroded surfaces).

Simulations have shown that the *field distribution inside the composite is highly inhomogeneous* in both phases (polymer matrix and ferroelectric particles).

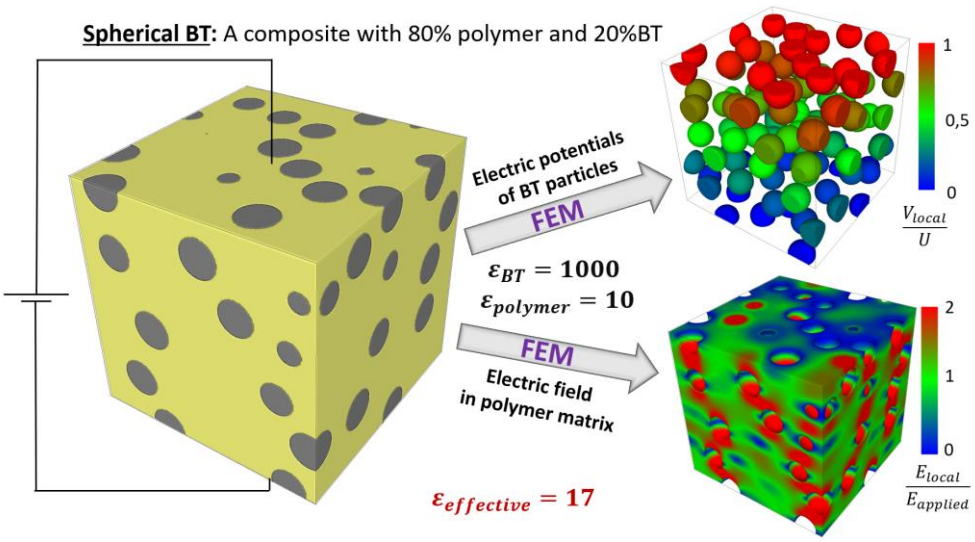

Figure 26. Simulation of local potential and fields and estimation of effective permittivity for a composite with 20% spherical BT nanoparticles within a polymer matrix.

For the same BT filler concentrations into the polymeric host matrix, it seems that there is a modest advantage of using cubic particles in increasing the permittivity of the composite: for a polymer permittivity of ε≈10 and ε≈1000 for $BaTiO_3$ inclusions, in the composite with 20% filler, an effective permittivity of ε≈19 (nanocubes inclusions) *vs.* ε≈19 ~17 (nanosphere inclusions) value is predicted. Even small for this combination of permittivity values, the increase is related to the property of field concentration in the corners and edges of the cube fillers.

In the next step, FEM simulations will be aimed to determine the role of: (a) the filler concentration; (b) the particle size and (c) the particle size distribution on the effective permittivity and compare the results with those reported in the literature for similar systems and results reported by using effective field models, as well as to estimate the permittivity enhancement produced by a synergic effect of BTO and metallic nanoparticle fillers.

2.7. The Design of Flexible Capacitors by Using $BaTiO_3$ Nanoparticles as Building Blocks

A schematic representation of the geometry in which these capacitors along with an image of a cross section of a thin layer of $BaTiO_3$ nanocubes are provided in Figure 28a. Figure 28b shows the graphs corresponding to the leakage currents on the surface unit of the dielectric thin layer, as well as the curve describing the dependence of the leakage current as a function of the applied voltage (J_{leak}-V). Preliminary data indicated the presence of a leakage current in the dielectric layers after the application of a voltage of 4 V (corresponding to a current density of (~8×10^{-5} A/cm^2), which suggests that these thin layers can operate in the range of voltage between 0 and 4 V. The dielectric polarization of this capacitor was measured according to the voltage applied at a frequency of 100 Hz. From the curve describing the behavior of the thin layer can be seen the presence of a nonlinear behavior, suggesting that the thin layer has ferroelectric

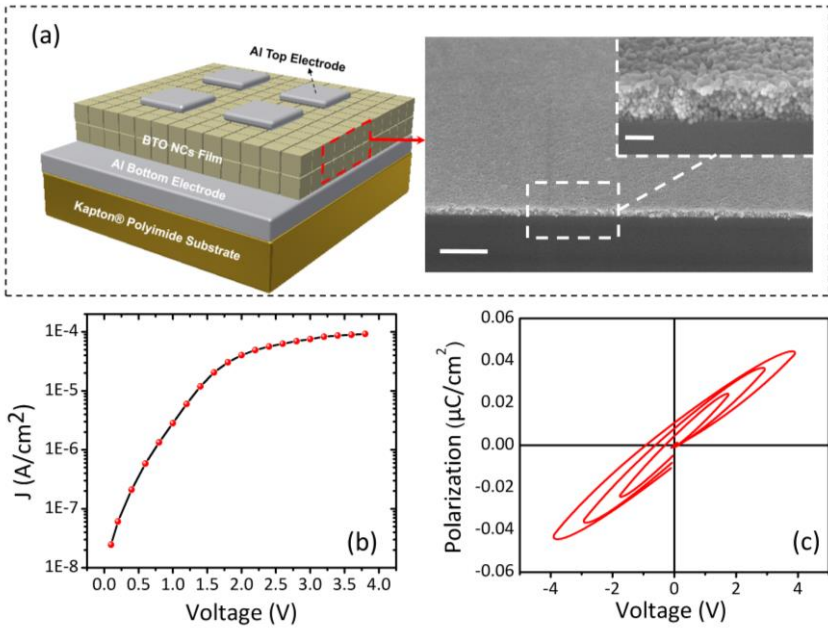

Figure 28. Diagram of a planar capacitor made of thin layers containing $BaTiO_3$ nanocubes with a size of 15 nm and the dielectric characteristics of this capacitor.

properties, with a residual polarization Ps of approximately 0.011 μC/cm^2 at a maximum voltage of 4 V. Another set of thin films have been obtained by NIMP partner. Thus, thin films were deposited on different rigid substrates, using as precursors BTO nanocrystals dispersed in a solvent. The solution was spread on the substrate by spin-coating. The obtained films were then analyzed by powder X-Ray diffraction (XRD), electron microscopy (TEM) and dynamic lattice analysis (Raman spectroscopy). Some thin film samples were deposited on MgO substrates for dielectric measurements in the microwave domain. Other films were prepared on Pt/Si substrate, with top contacts for electric measurements at low frequencies. Below are some TEM images of the films deposited on Pt/Si substrates. Furthermore, top metal contacts were deposited by sputtering and preliminary capacitance measurements were performed by varying the frequency and the bias voltage. An example of the C-V characteristics of the $BaTiO_3$ nanoparticle-based thin film is presented in Figure 29.

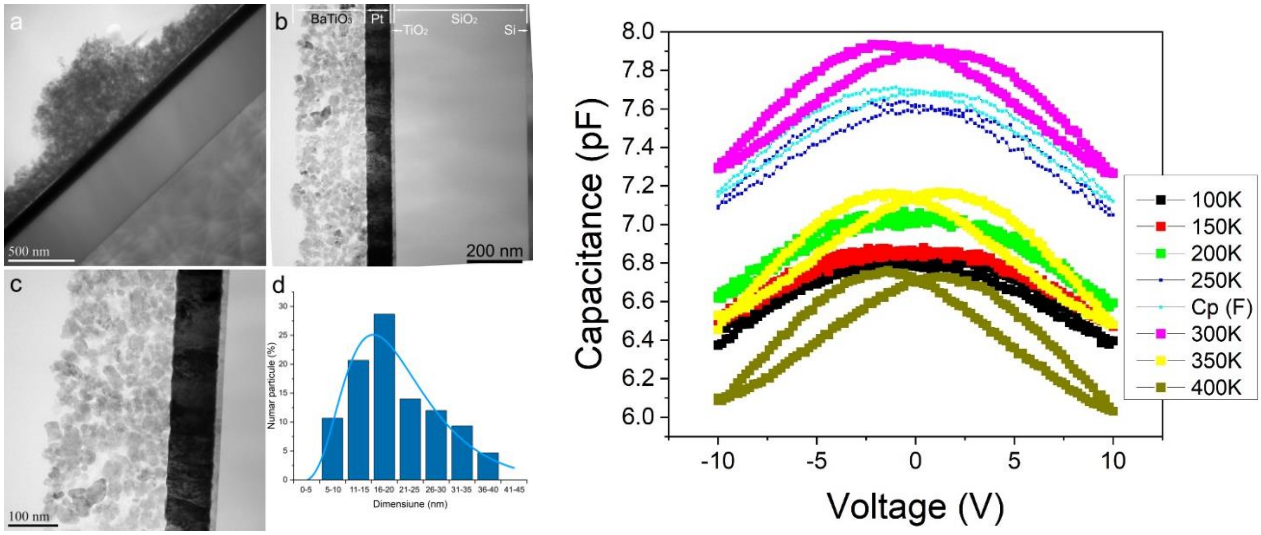

Figure 29. Conventional TEM images for a NC-$BaTiO_3$/Pt/TiO_2/SiO_2 structure (a-c); d) Size distribution plot of the $BaTiO_3$ nanoparticles fitted with a Log-normal function. The plot on the right side is an example of C-V characteristics of a capacitor made by using the $BaTiO_3$ nanoparticle film

Although this task is scheduled starting with Year 3, as our teams started since Year 2 to conduct exploratory experiments aimed at incorporating the dielectric films into field effect transistor devices.

2.8. Fabrication of $BaTiO_3$ Nanoparticle-Based Field Effect Transistors (FETs)

Below are presented relevant preliminary data related to the design of FETs by using close-packed nanoparticulate BTO films deposited on 50 μm polyimide flexible substrates (Kapton) The films were deposited from dielectric inks obtained by dispersing 15 nm $BaTiO_3$ nanocubes in toluene followed by drop casting and the slow evaporation of the solvent under ambient conditions. The semiconducting layer had an average thickness of 60 nm and consisted of a thin film made of spherical In_2O_3 colloidal nanocrystals obtained by a solution-based method, whereas the thickness of the dielectric film was about 100 nm. The FET was designed by depositing source and drain 50 nm Al electrodes by a thermal evaporation process upon a lift-off process. Figure 30 shows a picture of the dielectric ink containing 15 nm $BaTiO_3$ nanocubes (shown in the next picture as a top-down TEM image), a schematic of the FET and the image of the FET with a channel length ratio W/L of 10).

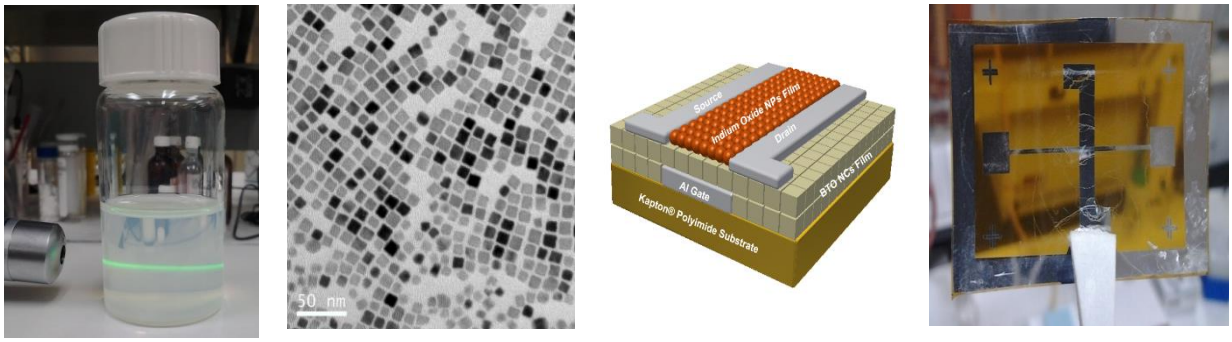

Figure 30. Dielectric ink containing 15 nm $BaTiO_3$ nanocubes (shown in the next picture as a top-down TEM image), a schematic of the FET and the image of the FET with a channel length ratio W/L of 10).

During Year 3 we will continue to design, model by finite element methods, characterize and optimize the FETs since the reproducibility of the experimental results is still problematic, due to the many variables involved in the fabrication of these devices. *As such, the design and testing/optimization of nanoparticle-based FETs is the highest priority of research for Years 3 and 4 and will involve the USV (fabrication of dielectric nanopowders/inks, dielectric spectroscopy and device design) UAIC (dielectric characterization and modelling) and NIMP (FET design, measurement, testing and modeling) partners.*

2.9. Optical properties investigated by THz spectroscopy

The THz experiments were performed by the INFLRP team (only this team possess such an experimental facility). TDS-THz spectroscopy has been used to investigate the dielectric properties of $BaTiO_3$. By measuring the amplitude and the phase of the transmitted and/or reflected waves by these samples the real and the imaginary constants of the material can be determined in the range of frequencies from 0.06 to 3 THz, respectively. The dielectric properties of $BaTiO_3$ nanoparticles of different sizes were investigated by THz spectroscopy under different ambient conditions. The samples consisted of nanoparticles dispersed in a nonpolar solvent, from which solid targets were fabricated, as well as BTO nanoparticles embedded in polymers. Spectroscopy investigations were performed (with a reasonable

noise) within the range of 0.3 to about 3 THz. As the main parameters used during these experiments we mention:

- Nanoparticle sizes between 0 to 30 nm
- A temperature range between 20^0 C and 100^0 C

Since there were investigations both in transmission and reflection (ATR -Attenuated Total Reflectance) for solid and liquid targets, pure nanoparticles, diluted in Toluene or embedded in polymer, the easiest comparison could be performed in between the refractive indexes (strongly bounded with the complex dielectric function) and this was the base of further results comparisons. The results were obtained with a 1 cm^{-1} resolution by mediating 1800 scan curves. For eliminating spectral noise produced by water vapors, sample chamber was purged by pure nitrogen (99.99999%) several minutes before each measurement.

2.9.1. Liquid Solution Terahertz Spectroscopy Measurements

$BaTiO_3$ nanoparticles spectroscopy experiments were performed in about 15 µl of liquid solution and used liquid medium was toluene. Investigations on concentration influences were showing an increase of the solution absorbance in the investigated spectral range, as expected. In Figure 31 is presented absorption variation in three representative ratios of nanoparticles (marked with 'X') of 0 wt. %, 30 wt. % and 100 wt. % respectively. The more particle in the solution, the more absorption of the sample, is the first conclusion from Figure 28. However, the solution absorption variation is not frequency independent, and so is the refraction index and respectively sample dielectric constant. As presented in Fig. 31, in the frequency range between 0.5 to 1.2 THz, the real part of the dielectric constant of the sample with a 30 wt. % of filler nanoparticles has a value intermediate between those of samples with a concentration of the filler x=0 wt. % and 100 wt. %, respectively. Outside of this range the dielectric constant of the sample with x= 30 wt. % has value which is bigger than those of the samples with x= 0 and 100 wt. %. These results suggest the existence of an optimal concentration of nanoparticle in the host polymer matrix from the dielectric performance viewpoint. From an application point of view could be summarized that the capacitive performance of a potential device will be maximized by a particular nanoparticle concentration. Since the optimal concentration is very likely to be a diluent dependent one and since the pure toluene is not going to be final application diluent, we concluded for now only the existence of an

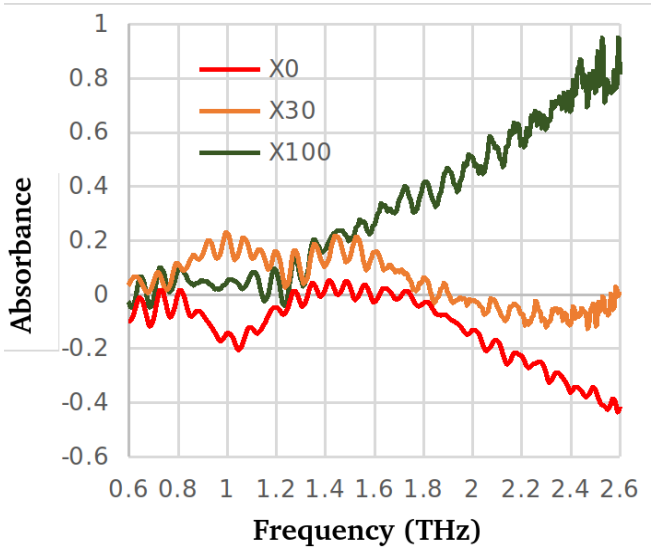

Figure 31. Variation of the absorbance of three different concentrations of 15 nm cuboidal $BaTiO_3$ nanoparticles concentrations

optimal concentration which in the case of toluene is around of 30 wt. % (with a precision several percent or but also depending on the targeted working frequency) (Figure 32).

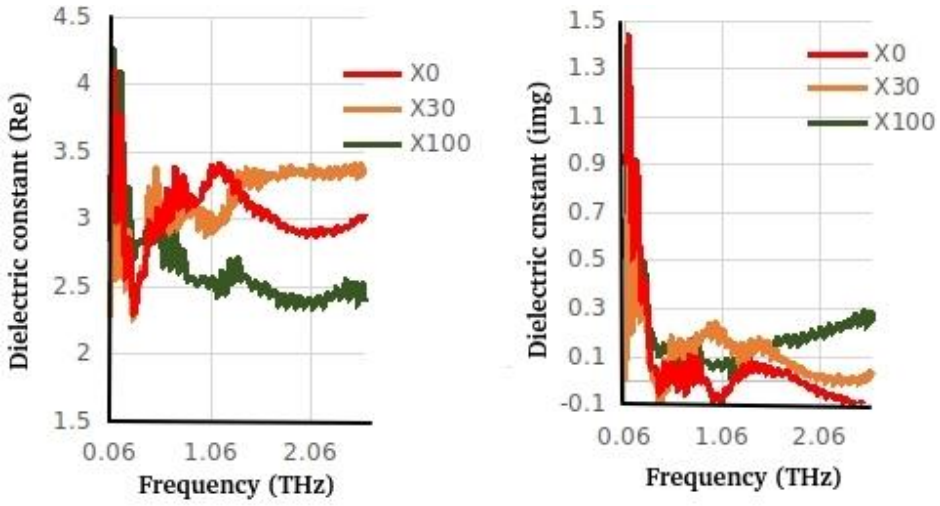

Figure 32. The frequency variation of the dielectric constant of 15 nm $BaTiO_3$ nanoparticles: (a) the real part and (b) imaginary part, respectively.

However, it worth to be mentioned that for the imaginary part of the dielectric constant (assigned to the dielectric losses) the 0.5–1.2 THz frequency range is corresponding to the band with the highest propagation losses, losses higher then both pure medium and pure nanoparticles in the same frequency domain. Complex refractive index coefficient variation (Fig. 19b) suggests that the X=30% concentration become efficient for frequencies above 1.5 THz. Based upon this value, it is reasonable to believe to be dependent on the diluent.

2.9.2. Solid Sample Terahertz Spectroscopy Measurements

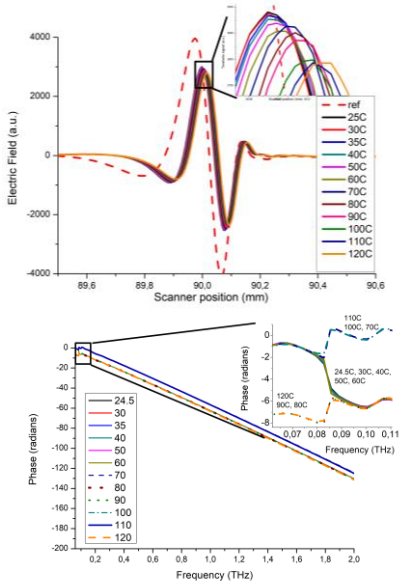

Figure 33. Temperature dependence of the time-domain signals of THz pulses in the presence/absence of the $BaTiO_3$

$BaTiO_3$ samples were obtained by compacting nanoparticle powders for 15 minutes by using a 5N force. Samples were tested in the temperature range from 20 to 120^0 C and the results in reflection mode (ATR) are presented below. As previously mentioned, the variation of the refractive index is directly proportional with the real part of dielectric constant variation and respectively consequently with capacitive performances of the sample). Variation of terahertz wave passing through the pellet samples and reflected back as compared with the reference-air (Figure 33, left plot) have shown a phase delay in the sample and changes of the THz signal amplitude with the temperature. The signal shift is more pronounced at higher temperatures (between 90 and 100 ^oC) while signal amplitude initially decreased with temperature between 25 and 60 ^oC and further increased around 70 ^oC, than decreased again and stabilized around

100 °C. This behavior is also visible on the phase change with (with about 6 radians) at the same temperature values: 70 °C, 80 °C, 100 °C and 120 °C. This could show that just changing the sample temperature the properties of $BaTiO_3$ nanoparticles could be changed. The phase change at each frequency directly yields the refractive index at each frequency, and signal amplitude change, combined with the refractive index variation, gives the absorption coefficient at each frequency. The refractive index and the absorption coefficients changes with temperature increase have been determined and are represented in Figure 34. The decrease of the refractive index is exponential decreasing with the temperature, while the absorption coefficient increased with temperature, possibly due to the free carrier absorption.

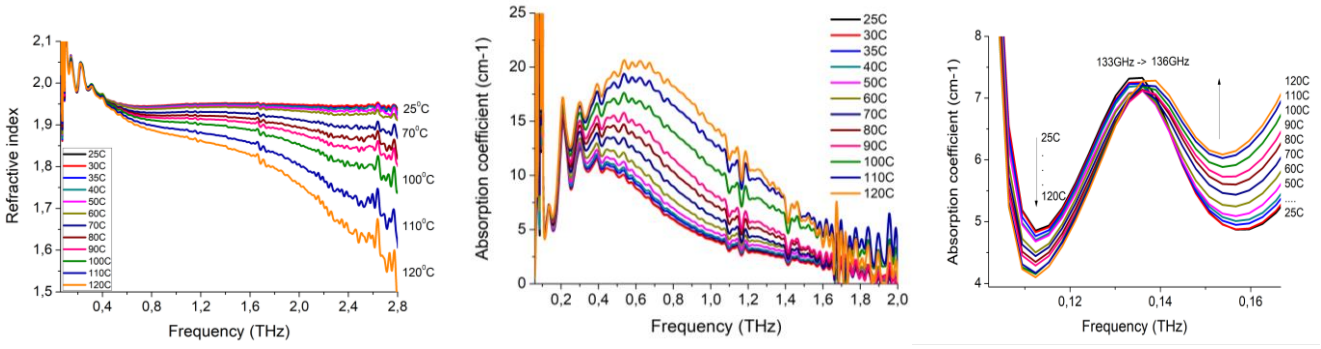

Figure 34. Frequency dependence variation with temperature of the refractive index (left plot); absorption coefficient (middle plot) and a zoomed image of the absorption coefficient frequency shift (right plot).

A more detailed investigation of the variation is presented in Figure 34 (left plot) for the spectral ranges of 0.21–0.24 THz where a shift toward smaller frequencies of the refractive index peak is induced by the increase of the sample temperature. Similar observation could be made for the 0.3 – 0.32 THz peak in the plot in the middle of Figure 35). A consequence of the shifts is an opposite temperature variation trend of the refractive index (and respectively dielectric coefficient) for a particular range of frequency.

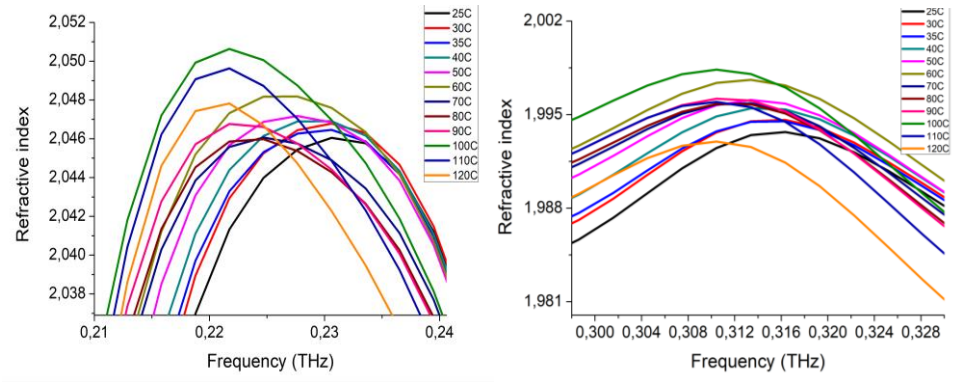

Figure 35. Refractive index peaks shift with the temperature increase within the a) 0.21 – 0.24 THz and b) 0.3 – 0.32 THz.

An example is presented in Fig 36 for two relatively close frequencies of 0.24 THz and respectively 0.28 THz. From applicative point of view, the capacitive performances of the device based on such samples might have opposite variation trends with temperature for relatively close working frequencies.

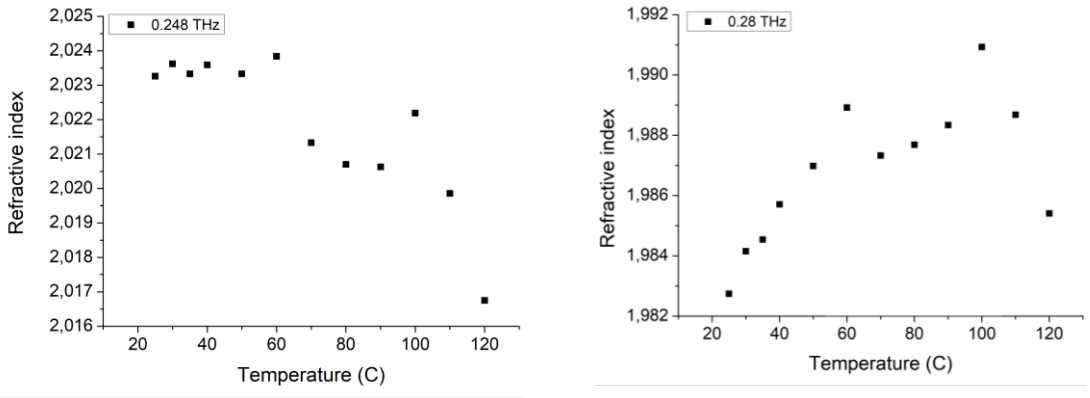

Figure 36. Refractive index temperature dependence at: a) 0.248 THz and b) 0.28 THz

Further investigations on the phase shift with temperature are under development, and checks on the dielectric properties switching reproducibility.

2.9.2. Terahertz Spectroscopy Measurements of Polymer-Ceramic Nanocompoosite (Activity 1.3.1 and 3.2.3)

$BaTiO_3$ nanoparticles of different sizes were mixed in different concentrations in SBS polymer and dielectric parameters were measured in the same conditions described above. Concentration influence of 20 nm $BaTiO_3$ on polymer refraction index at room temperature is presented in Figure 37. As a first impression, the concentration strongly influences the absorption parameter (as also observed for solutions) as well as refractive index (and consequently dielectric constant) variation. However, it is interesting to note that the mass concentration is not the dominant factor. Thus, a smaller nanoparticle size will produce a stronger decrease of the refractive index then a bigger particle for similar mass concentration. In Figure 38, is exemplified the for 10% mass concentration of 10 nm and 20 nm nanoparticle respectively, in SBS. The above results might somehow induce the idea that "bulk" capacitive performances would be the best. However, previous results in solutions were suggesting the existence of an optimal concentration rather than a continuous variation. While mass concentration is certainly not the representative parameter according to Figure 36, we decided to test several nanoparticle sizes at several concentrations and respectively temperatures. Starting from the specific volume of a SMS moll and evaluating the specific nanoparticle surface corresponding to each mass concentration used, we obtained the graphs from Fig. 38

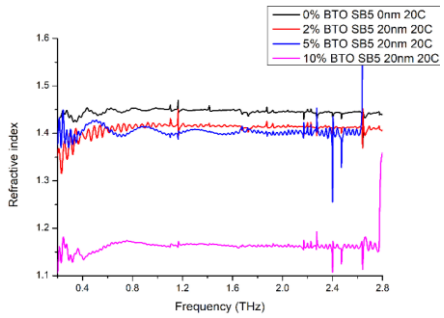

Figure 37. Refractive index value is constantly decreasing with the increase of the nanoparticles concentration for the whole investigated frequency range.

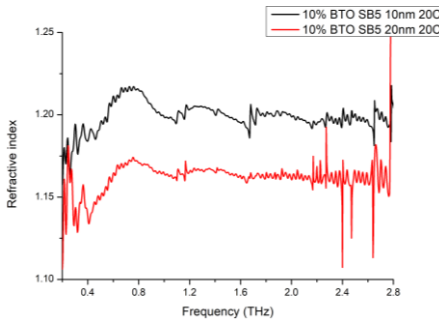

Figure 38. SBS refractive index variation for 10 wt. % BTO concentration of different sizes

for different working temperatures. It could be seen that around 6 nm^2 /SBS moll (Fig. 39a) refractive index apparently has a peak which is almost frequency independent for our investigated frequencies. The peak still has a relatively week temperature dependence (which means a variation below 10% of the capacitive performances of a device for a temperature variation of about 80^0 C). One can also notice that samples with specific surfaces seems more sensitive to some higher temperatures as it is the case of the 30 nm^2 / SBS moll sample at 100^0 C at working frequencies above 1.4 THz (Fig. 26 b and c).

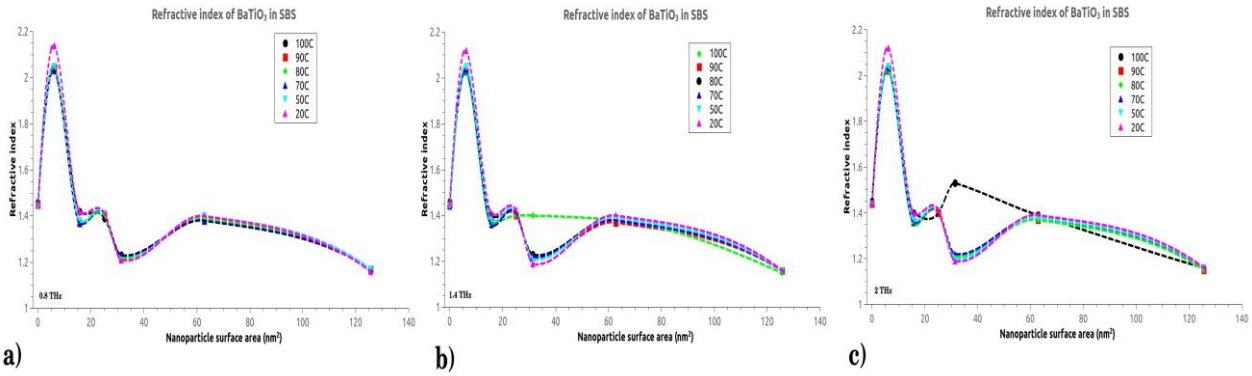

Figure 39. Refractive index variation with nanoparticle specific are in SBS, at different temperatures, at working frequencies of a) 0.8 THz, b) 1.4 THz and c) 2 THZ

3. Progress Beyond the State of the Art and Expected Results Until the End of the Project

The results obtained in during the first two years of the research project, despite the inherent difficulties due to waiting times for the delivery of chemicals, supplies and scientific instrumentation, as well as the Covid-19 pandemic unquestionably demonstrate that a substantial progress has been made by each partner teams towards the completion of specific tasks and activities converging to the integration of nanoparticulate $BaTiO_3$ dielectric films into both active (FETs) and passive (capacitors) electronic devices. Below are summarized the main achievements during the first two years and underlined the activities to be performed during the next two years of the project:

I. Complete the systematic investigation of the dielectric and ferroelectric properties of $BaTiO_3$ films

Films with different thicknesses have been and will be fabricated by assembling individual cuboidal $BaTiO_3$ nanocrystals with different sizes and their properties will be characterized. Preliminary measurements of these film structures revealed that the value of the dielectric constant can be tuned depending on both the size of the nanocubes, the nature of the capping agent which passivates their surface and porosity level. *The results obtained from these measurements will be benchmarked against the properties of nanoparticle-based dielectric films obtained by other groups and thin films obtained by physical and chemical deposition*. Since we are able now to reproducibly synthesize ferroelectric $BaTiO_3$

nanoparticles with tunable properties, we will self-assemble these nanoparticles into films and membranes in the presence of an external electric field. Such type of assemblies were fabricated in the case of magnetic nanocrystals but they were not fabricated in the case of dielectric/ferroelectric nanoparticles. We anticipate that the self-assembly of the ferroelectric cuboidal nanoparticles would lead to film and membrane structures which have even higher dielectric constant values, as the face-mediated self-assembly of the nanoparticles will take advantage of an epitaxial-like growth between adjacent nanocubes and their flat , defect-free surfaces.

II. Design of $BaTiO_3$-Polymer Dielectric Films

We have selected polypropylene (PP) or poly(vinylidene fluoride-co-hexafluoropropene) (P(VDF)-HFP) to fabricate dielectric nanocomposite films and membranes by using the solution-based method developed by our team. After fabricating these nanostructures, we will measure their dielectric/ferroelectric properties and compare them with those of $BaTiO_3$-based thin films. The polymers selected by NIMP and USV teams will complement those used by the UAIC team to avoid any overlap in the work and delay in completing the activities related to this objective. As it happened during the first two years of the project, the experimental results will be shared between teams in order to identify the polymer-ceramic nanostructures with the best dielectric characteristics for integration into devices. It is expected that the integration of a polymer into the nanocomposite films/membranes will add a degree of freedom to these structures; that is flexibility, which is highly desired for the design of flexible dielectrics for electronics. Preliminary work performed by our teams on the rational design of substrate-free polymer ceramic nanocomposite films consisting of differently sized (10 nm and 20 nm), oleic acid-coated $BaTiO_3$ colloidal nanocrystals dispersed into styrene butadiene styrene (SBS) has shown that such nanocomposites have dielectric properties that can rival those of the $BaTiO_3$ films obtained by conventional physical deposition methods, with dielectric constant values ε=34 upon incorporating 10 nm and 20 nm $BaTiO_3$ nanocubes into the elastomer matrix. experimental values of the dielectric permittivity and those calculated by using different binary composite models (Lichtenecker, Bruggeman and modified Kerner). To this end, we will continue in the next two years of the project to model the dielectric properties of baTio3 nanoparticles and $BaTiO_3$-based polymer-ceramic nanocomposites by using effective medium approximation (EMA) and finite element (FEM) methods to (1) study the role of the porosity on the dielectric properties of these films and (2) determine the maximum volume fraction of nanocrystals achievable avoiding the creating of voids and the formation of dense films.

Along with the dielectric characterization of the films and membranes, a systematic study of the role of different mechanisms (Maxell-Wagner, interfacial polarization, etc.) and surface absorbents on the polarization as well as the influence of the electrode polarization on the dielectric permitivity will be performed. To this end, capacitors incorporating dielectric films in tandem with electrodes having different

work functions, including Ag, Cu and Au will be fabricated and tested , the most promising films being incorporated into field effect transistors on both rigid and flexible substrates.

III. Design of Capacitor and Field-Effect Transistor Structures by Using Nanoparticle-Based or Polymer-Ceramic Nanoparticle Films/Membranes as Dielectric Layer

In the next steps, we will fabricate dielectric films by either casting $BaTiO_3$ nanoparticle-based inks onto both rigid and flexible substrates or fabricating polymer-ceramic or ceramic films/membranes by a solution-based deposition method developed. The properties of these nanostructures will be tested and optimized by studying the variation of the effective dielectric permittivity, dissipation factor, normalized capacitance, electric displacement, and leakage current density-voltage and conductivity of the nanoparticle-based and nanocomposite films in different frequency and temperature ranges and as a function of the concentration of the nanofillers. In parallel, the resistance to short-circuits of these nanostructures will be tested by breakdown strength measurements and the potential gain of energy density will be assessed by performing Weibull statistics. To these dielectric films metallic electrodes will be attached by using lithography and/or metal evaporation methods, which will enable the design of planar capacitor structures (both rigid and flexible). The characteristics of the capacitors will be measured and optimized, as a function of various parameters, including:

- the size of the nanoparticles making up the dielectric films;
- the porosity of the films;
- the nature of the metallic electrode, etc.

A particular attention will be paid to the non-linear characteristics of the capacitors, expected to arise from the ferroelectric properties of the $BaTiO_3$ nanocrystals, which make these capacitors attractive for energy storage applications. The dielectric layers will be also integrated into field effect transistor (FET) devices using flexible substrates followed by the measurement and optimization of their output and transfer characteristics. To this end, different semiconductors (polymer or ceramic) layers will be used, the ultimate goal of the project being the design of an „all inorganic" FET, in which the dielectric layer is made of $BaTiO_3$ colloidal nanocrystal films and the semiconductor layer is an oxide (such as TiO_2, In_2O_3, etc.) material, in the form of nanocrystals. Different combinations of materials and device geometries will be tested to enable the operation of FETs at low voltage with minimal switching reversibility without sacrificing the charge mobility in the semiconducting channel. In parallel, a comprehensive study of the charge transport and trapping mechanisms and their dependence on the semiconductor/dielectric interface will be performed. The ultimate goal is to establish a relationship between the morphology and surface chemistry of the dielectric and semiconductor nanocrystals and the performance and switching reversibility of the FETs as a function of the interface trapped-state density. Similar to the capacitor structures, the performance of FETs obtained by integrating the dielectric nanoparticle-based films will be benchmarked

against the characteristics of different devices fabricated by other groups and reported in the literature integrating nanoparticulate dielectric and semiconductor materials.

IV. Multifunctional Ceramic Composites Based on $BaTiO_3$ Nanoparticles Combined with Spinel Ferrite Nanoparticles

$BaTiO_3$ nanopowders were used to produce high quality multifunctional composites, *i.e.* ferroelectric-ferrite magnetoelectric biphasic composites with optimized micro/nanostructures, controlled phase connectivity and grain size. We performed an analysis of the role played by the phase connectivity on the properties of composites, as well as a comparative study of the direct magnetoelectric effect (ME) on 3-3 *vs.* 2-2 magnetoelectric nanocomposites was demonstrated by studying the variation of their properties (linear dielectric, conductivity, dispersion in frequency, high field properties as ferroelectric P(E) and tunability, microwave characteristics). We demonstrated for the first time that $BaTiO_3$-$Co_{0.8}Zn_{0.2}Fe_2O_4$ composites possess a bi-tunable character, *i.e.* a variation of their dielectric permittivity both under the action of *dc* electric and *ac* magnetic fields. The ability of these nanocomposites to shift the resonance of a major magnetic mode (TEme010) under dc magnetic field as result of magnetoelectric coupling make these composites very attractive for applications in microwave filters. Until the end of the project, the design of such a device will be completed and the device will be tested under different conditions. If appropriate, a proposal for a national patent will be submitted or if necessary, the submission of a proposal for an applied-science research grant, together with a SME Romanian company and team partners in the current project, will be considered.

V. $BaTiO_3$ Porous Ceramics from Cuboidal Nanoparticles for Gas Sensing:

We demonstrated the ability to produce $BaTiO_3$-based nanostructured ceramics with a high porosity level around the percolation limit (33%, 37% relative porosity) by using field-assisted fast sintering. Upon optimization of the sintering parameters, a high porosity was reached together with a good mechanically stability, and preserving the initial morphology of the cuboidal nanograins into the consolidated product. *This represents a significant novel result at international level*. The resulted ceramics have cube-like grains of a size ranging between 10 and 40 nm, with regions of self-assembled nanocubes and a multiscale porosity level ranging from a few nm^3 cubic pores to hundreds of nm^3. Around room temperature he dielectric response is dominated by a prominent interface-driven Maxwell-Wagner conductivity relaxation, which is related to the gas and adsorption of water molecules at the porous ceramic interfaces. This feature indicated a potential high room temperature sensitivity of the electrical properties to interface-driven phenomena, namely the adsorption of gas molecules at the ceramic-pore interfaces. This hypothesis was validated by performing preliminary gas sensing tests in dynamic regime, at normal room temperature and pressure conditions, using acetone as testing gas. Research on designing and testing nanoparticle-based gas sensing

devices is new for the UAIC group and these activities were performed by using semiconductor NiO structures during the first year of the present grant. Porous $BaTiO_3$ ceramics with nanoscale cube-like grains show a high level of replicability under repeated cycles of testing and a higher sensitivity at lower frequencies for both real and imaginary part of their impedances. Further studies will be aimed to determine the sensitivity and selectivity of these nanostructures towards other volatile species, as well as the study of their response time characteristics.

VI. Fabrication and Testing of Flexible $BaTiO_3$-Based Composites

Calculations based on 3D Finite Element Methods (FEM) applied to composites made of a low-permittivity host polymer matrix incorporating high permittivity ferroelectric nanoparticles, such as $BaTiO_3$ shown how the electric field and the electric potential are distributed within the composite with respect to both phases (polymer matrix and ferroelectric particles). *This result alone, is new and significant.* By performing simulations for composite materials incorporating $BaTiO_3$ filler nanoparticles with two different types of shapes (cubic and spherical) and preserving the other characteristics (the same concentration of the filler, the same polymeric matrix, etc.) a modest advantage of the use of cubic particles *vs*. spherical ones was observed in an attempt to identify the type of composite with the maximum value of the dielectric permittivity. For a polymer host matrix with a value of the dielectric permittivity $\varepsilon=10$ and a dielectric constant of the $BaTiO_3$ fillers $\varepsilon=1000$, the corresponding composite with a concentration of the BTO filler of 20 wt.% and the filler nanoparticles randomly distributed, the value of the effective calculated permittivity was $\varepsilon=19$ (for cuboidal inclusions) *vs.* $\varepsilon=17$ (for spheroidal inclusions), *This result alone, is new and significant*. Although such an increase seems to be modest, for some specific configurations it could be enhanced as result of the concentration of the electric field at the corners and edges of cuboidal fillers, thereby enhancing the dielectric effective response of the composite. In the first years of this project, flexible composites containing $BaTiO_3$ cube-like fillers dispersed into various polymer matrices (PVDF, epoxy resin, PCL or gelatin biopolymer) were fabricated by solution casting. With respect to the experimental part, one of the interesting novel results is the use of a non-toxic gelatin as a polar biodegradable host matrix in which ferroelectric 10 nm $BaTiO_3$ nanocubes were dispersed at concentrations up to 40 wt. %. An increase of the permittivity from $\varepsilon=9$ (in pure gelatin) to $\varepsilon=15$ (40 wt. % BT) and dielectric losses below 5% were observed at a frequency of 10^5 Hz for these composites. Promising results concerning the electrostatic energy storage capacity of such flexible capacitors indicate an optimum behavior for filler concentrations of 18 wt. %. Therefore, this system should be further optimized and investigated in detail.

VII. Structural Characterization of $BaTiO_3$ Nanopowders

Experimental evidence of an anisotropic strain, leading the broadening of the XRD lines, was explained by the existence of surface relaxation; that is the increase of the lattice constant towards the surface of the BTO nanocubes. The effects of nonpolar oleic acid (OA) and polar tetrafluoroborate (BF_4^-) ligand capping on the surface of various sizes of $BaTiO_3$ nanocubes were investigated by combining advanced structure characterization techniques, such as neutron diffraction and neutron pair distribution function (PDF), density functional theory (DFT), and *ab initio* molecular dynamics (AIMD) methods. The low real space PDF region provides an unobstructed view of rhombohedral (split short and long) Ti-O distances in $BaTiO_3$ nanocubes, mimicking the well-established order-disorder local structure found in bulk $BaTiO_3$. Interestingly, the intermediate-range order in nanocubes is found to be orthorhombic, rather than tetragonal. We conclude that polar ligands adsorbed at $BaTiO_3$ surfaces stabilize the correlation length scale of local rhombohedral distortions in ferroelectric nanoparticles relative to nonpolar ligands.

VIII. Optical properties investigation by THz spectroscopy

Preliminary results were obtained for polymer-ceramic composites with different volumetric or mass concentrations of the filler nanoparticles. These results suggest that the filler concentration alone is not sufficient for characterizing the refractive index of these materials. With respect to the influence of temperature on the refractive index of polymer-ceramic composites we noticed that some of the peaks decreased in intensity when temperature increased. For higher specific surface area of the BTO filler nanoparticles, an increase of the refractive index was observed, especially at higher temperatures. Even if the tendency could be tentatively ascribed to the thermal degradation of the polymer, it is worth noting that this variation depends on the concentration of the filler nanoparticles. In the case of BTO-SBS composites, room temperature could induce significant variations of the value of the dielectric constant. Remarkably, these variations are not strictly dependent on the polymer parameters but rather on the parameters of the polymer host matrix. Thus, we observed that the increase of the temperature induces a decrease of the refractive index at small concentrations (2 wt. %) of nanoparticles, whereas an opposite effect was observed for higher concentrations (10 wt. %) of the filler nanoparticles. Further work on this project will be focused on temperature-dependent terahertz spectroscopy of variably-sized $BaTiO_3$ nanoparticles, in order top map the order-disorder phase transitions associated with the onset/eradication of ferroelectricity in these systems and the experimental determination of their dielectric constant values.

3. Results Indicators

Indicators	Description / Name	No.
Articles published/accepted/under evaluation in ISI indexed journals	*Article title/Year/DOI/ISSN or eSSN/Journal/ Authors/ Status (under evaluation/accepted/published)*	
	1. Functional properties of randomly mixed and layered BaTiO3 - CoFe2O4 ceramic composites close to the percolation limit; 2019; https://doi.org/10.1016/j.jallcom.2019.05.068; ISSN: 0925-8388**; Journal of Alloys and Compounds** 796, 55-64; A. Guzu, C.E. Ciomaga, M. Airimioaei, L. Padurariu, L.P. Curecheriu, I. Dumitru, F. Gheorghiu, G. Stoian, M. Grigoras, N. Lupu, M. Asandulesa, L. Mitoseriu (published) 2. Comparative study of magnetoelectric BaTiO3–Co0.8Zn0.2Fe2O4 bi-tunable ceramics sintered by Spark Plasma Sintering and classical method; 2019; https://doi.org/10.1016/j.ceramint.2019.08.125; ISSN: 0272-8842; **Ceramics International** Vol. 45, Issue 18, Part A, 24168-24175; C.E. Ciomaga, A. Guzu, M. Airimioaei, L.P. Curecheriu, V.A. Lukacs, O.G. Avadanei, G. Stoian, M. Grigoras, N. Lupu, M. Asandulesa, L. Mitoseriu (published) 3. Biomorphic tubular nickel oxide structures: effect of the synthesis parameters on their structural and functional properties, surface-related applications; 2020; https://doi.org/10.1016/j.jallcom.2019.152543; ISSN: 0925-8388; **Journal of Alloys and Compounds** Vol. 816, 152543; M. Airimioaei, V.A. Lukacs, I. Lisiecki, P. Beaunier, J. Blanchard, D. Lutic, S. Tascu, P. Postolache, C.E. Ciomaga, M. Olariu, L. Mitoseriu (published) 4. Four-fold multifunctional properties in self-organized layered ferrite; 2020; https://doi.org/10.1016/j.ceramint.2020.08.021; ISSN: 0272-8842; **Ceramics International** vol. 46, 28621–28630; L. Curecheriu, C. Harnagea, M.T. Buscaglia, I. Pallecchi, B.S. Vasile, V.A. Surdu, A.C. Ianculescu, A. Pignolet, F. Rosei, L. Mitoseriu, V. Buscaglia (published) 5. PVDF–ferrite composites with dual magneto-piezoelectric response for flexible electronics applications: synthesis and functional properties; 2020; https://doi.org/10.1007/s10853-019-04279-w; Electronic ISSN: 1573-4803, Print ISSN: 0022-2461; **Journal of Materials Science** vol. 55, 3926–3939; F. Gheorghiu, R. Stanculescu, L. Curecheriu, E. Brunengo, P. Stagnaro, V. Tiron, P. Postolache, M.T. Buscaglia, L. Mitoseriu (published) 6. Improved dielectric properties of poly(vinylidene fluoride)–BaTiO3 composites by solvent-free processing; 2021, https://doi.org/10.1002/app.50049; Print ISSN: 0021-8995, Online ISSN: 1097-4628; **Journal of Applied Polymer Science** vol. 138, issue 12, 50049; E. Brunengo, L. Conzatti, I. Schizzi, M.T. Buscaglia, G.	*15*

	Canu, L. Curecheriu, C. Costa, M. Castellano, L. Mitoseriu, P. Stagnaro, V. Buscaglia (published) 7. Effect of $BaCO_3$ Impurities on the Structure of BaTiO3 Nanocrystals: Implications for Multilayer Ceramic Capacitors https://pubs.acs.org/doi/10.1021/acsanm.0c01809 **ACS Applied Nano Materials**,Volume: 3 Issue:10 Pages:9715–9723 DOI: 10.1021/acsanm.0c01809 Tedi-Marie Usher, Benard Kavey, Gabriel Caruntu, Katharine Page (published) 8. Dielectric properties of solution-processed BaTiO 3–styrene butadiene styrene nanocomposite films **CrystEngComm**,Volume: 22 Issue:7 Pages:1261-1272, DOI:10.1039/C9CE01912J Daniela Caruntu, Benard Kavey, Suporna Paul, Alin Ciprian Bas, Aurelian Rotaru, Gabriel Caruntu (published) 9. Varistor and Electrical Properties of MgO.(Fe2O3)1-x(Bi2O3)x Ceramics **Journal of the European Ceramic Society**, Volume: 40 Issue:4 Pages:1325-1329, DOI:10.1016/j.jeurceramsoc.2019.11.084 Niousha Varastegani, Amin Yourdkhani, Seyyed Ali Seyyed Ebrahimi, Aurelian Rotaru (published) 10. Preparation and properties of porous BaTiO3 nanostructured ceramics produced from cuboidal nanocrystals **Ceramics International** Vlad Alexandru Lukacs; Gabriel Caruntu; Oana Condurache; Cristina Elena Ciomaga; Lavinia Petronela Curecheriu; Leontin Padurariu; Maria Ignat; Mirela Airimioaei; George Stoian; Aurelian Rotaru; Liliana Mitoseriu **(accepted) – 2021 (in press)** https://doi.org/10.1016/j.ceramint.2021.03.128 11. Effect of Ligand Polarity on the Internal Dipoles and Ferroelectric Distortion in BaTiO3 Nanocubes **Chemistry–A European Journal** Jiang, Bo; Usher, Tedi-Marie ; Jothi, Palani Raja; Benard, Kavey ; Caruntu, Gabriel; Page, Katharine **(accepted) - 2021 (in press)** https://doi.org/10.1002/chem.202100692	

	12. Magnetic and electrical properties of $Mg_{1-x}Co_xFe_2O_4$ (x=0-0.15) ceramics prepared by solid state method **Journal of the European Ceramic Society** Maryam Nili-Ahmad-Ababdi; Amin Yourdkhani; Andrei Diaconu; Aurelian Rotaru **(submitted / under evaluation)** 13. The effects of sintering temperature on structural, electrical, and magnetic properties of MgFe1.92Bi0.08O4 Ferrites **Journal of Electroceramics** Niousha Varastegani, Amin Yourdkhani, Seyed Ali Seyed Ebrahimi, Aurelian Rotaru **(submitted / under evaluation)** 14. Insights into Structural, Optical, and Catalytic Properties of MgCr2O4 Spinel-type Nanostructures Synthesized by Sol-Gel Auto-Combustion Method. **ACS Applied Nano Materials** V. Mykhailovych, A. I. Kanak, Ş. Cojocaru, E.-D. Chitoiu-Arsene, M. N. Palamaru, A.-R. Iordan, O. O. Korovyanko, A. Diaconu, G. Caruntu, O. V. Lushchak, P. M. Fochuk, Y. B. Khalavka, A. Rotaru **(submitted / under evaluation)** 15. In-situ TEM Measurement of Electrical Properties of Individual BaTiO3 Nanocubes", **Applied Physics Letters** Tian, Xinchun, Caruntu, G. Kavey, B. and Xiaoli Tan **(submitted / under evaluation)**	
Articles published/accepted/under evaluation in BDI indexed journals	*Article title/Year/Journal/Authors/Status(under evaluation / accepted/published)*	
Patent applications filed nationally and internationally	*Patent title/Issuing authority/Submission date*	
Patents obtained at national and international level	*Patent title/Issuing authority/Issue date*	
Conferences attendance	*Conference name/Type/Title/Year* **1)** G. Caruntu, B. Kavey, D. Caruntu , A. Rotaru **"** *Solution-processed ferroelectric perovskite colloidal nanocrystals for application in electronics and data storage*", **16th International Conference on Nanosciences and Nanotechnologies (NANOTEXNOLOGY), Salonic, Greece , 2019 (oral presentation)** **2)** Aurelian Rotaru**"** *Nanoelectronic and spintronic devices based on molecular spin crossover materials*", **16th International Conference on Nanosciences and Nanotechnologies (NANOTEXNOLOGY), Salonic, Greece , 2019 (oral presentation)** **3)** D. Caruntu, J. Lentz, G. Caruntu „Rational Design of 1D Cobalt Ferrite Nanostructures by Liquid Phase Deposition", **16th International Conference on Nanosciences and Nanotechnologies (NANOTEXNOLOGY), Salonic, Greece , 2019 (poster)**	15

	4) F. Gheorghiu, L. Curecheriu, E. Brunengo, L. Mitoseriu "*The Synthesis and Characterization of PVDF-Based Composites for Flexible Electronics*", **F2Cp2 Conference, Laussane, Elvetia, 2019 (poster)** **5)** M. Airimioaei, A. Lukacs, I. Lisiecki, P. Beaunier, C. Ciomaga, L. Mitoseriu „*Structural and Functional Properties of Biomorphic Tubular NiO Structures"* **F2Cp2 Conference, Laussane, Elvetia, 2019 (poster)** **6)** C. Ciomaga, M. Airimioaei, A. Guzu, F. Gheorghiu, G. Stoian, M. Grigoras, M. Asandulesa, L. Padurariu, L. Mitoseriu, **„***Comparative Study of the Functional Properties for Mixed and Trilayered BaTiO3-Based Magnetoelectric Composites"***, F2Cp2 Conference, Laussane, Elvetia, 2019 (poster)** **7)** Ioana Pintilie, „*Functional properties of BaTiO3-based ceramics, thin films and nanostructures*", **Sustainable Industrial Processing Summit & Exhibition, Paphos, Cyprus 2019 (poster)** **8)** Marcu Aurelian, „*Laser Grown Oxide Nanowire Layers*", **Sustainable Industrial Processing Summit & Exhibition, Smart NanoMaterials 2019 - SNAIA2019, Paris, France 2019 (oral presentation)** **9)** T. Costanzo, G. Caruntu **„***Size Dependency of the Ferroelectric Properties in Single Nanocrystals of BaTiO3 Locally Investigated by HRTEM and PFM***", Materials Research Society (MRS) Spring Meeting, April 22-26, 2019 (oral presentation)** **10)** S. Paul, B. Kavey, G. Caruntu **"***Fabrication, Characterization and Dielectric Spectroscopy of BaTiO3 Styrene Butadiene Styrene Stretchable Thin-Film Nanocomposites for Flexible Electronics***" Materials Research Society (MRS) Spring Meeting, April 22-26, 2019 (poster)** **11)**B. Kavey, D. Caruntu, A. Rotaru, G. Caruntu, **"***Fabrication and Characterization High-k BaTiO3 Colloidal Nanocrystals and Nanoparticle-Based Thin-Films***", Michigan Microscopy and Microanalysis Society (MMMS) Annual Meeting, October 29, 2019, Ann Arbor (MI), USA (poster)** 12)B. Kavey, D. Caruntu, A. Rotaru, G. Caruntu, *"Controlled Synthesis and Electromechanical Characterization of Europium-Doped BaTiO3 Nanocrystals: Implications in Energy Harvesting, Storage and Transfer", **Materials Research Society (MRS) Fall Meeting (Virtual)**, November 27-December 4, 2020* ***(Prezentare orala)*** 13)A. Marcu, R. Mihalcea, A. Stancalie, C. Viespe, and N. Ionut, *"OxideNanostructure Growing for Sensors Applications"*, **6th BiennialInternational Conference on Emerging Trends in Engineering Science and Technology - ICETEST2020**, 17 - 19th December 2020, Thrissur, India ***(Invited)*** 14)Aurelian Marcu, Razvan Mihalcea, C. Samoil, E. Slushanschi, V.Chihaia, I. Nicolae and C.Viespe, *"ZnO Nanostructures for Gas Sensing"*, SNAIA 2020, *8-11 December 2020*, Paris, France ***(Prezentare Orala)*** 15)L Mihai, A. Marcu, A. Rotaru, G. Caruntu, D. Caruntu, A. Stancalie and M. Ghena, *"BaTiO2 Dielectric Properties in Polimers"*, **Emergemat 3rd International Conference On Emerging Technologies In Materials Engineering**, 29-30 October 2020, Bucharest, Romania ***(Prezentare poster)***	
Books	*Title/Publishing year/Publishing house/ISBN*	

Book chapters	*Book title/chapter title/Publishing year/Publishing house/ISBN*	
Other results	**Networking:** Realisation of active collaboration with CO group: using their BT nanocube-like powders to realise composite and porous ceramics, exchange of samples, ideas and modeling results, using the CO facilities for Raman, DSC analyses, etc.	

4. Equipment Use

(for the equipment purchased from the project and whose value exceeds 60.000 lei will be briefly described how they are used to meet the objectives of the project).

USV: High Temperature/High pressure rector systems have been used for hydrothermal synthesis of $BaTiO_3$ nanoparticles.

Electrometer with high voltage source and TSDC sample cell has been used for DC electrical characterization and thermal stimulated depolarization currents analysis.

Ferroelectric tester (FE – Module (integrator) with preinstalled High voltage protection for use with HV amplifiers up to 10kV• FE Probe Head• Frequency 0.01Hz – 1MHz @12V hysteresis measurements (integrator ranges)• aixPlorere3.0 measuring software for FE-Module, Piezoelectric Characterization Module; C(V) measurement Module; TFSHU- Thin Film Sample Holder Unit) used for measurements of ferroelectric and piezoelectric properties, Temperature module: -196 ^{o}C– 600 ^{o}C.

UAIC: Precision Multiferroic and Ferroelectric Test System (Test Stations, 10kV High Voltage Testing, Thermal Testing, Piezoelectric, Pyroelectric, Magnetoelectric Testing, Vision Software), Radiant Technologies Inc., Albuquerque, NM, USA – used for the measurements of ferroelectric and non-linear dielectric properties: tunability, P(E), magnetoelectric coupling.

NIMP: Optical microscope-it is used to inspect the contacts, layers, devices, in a clean room environment.

Cutting machine with disk-it is used to cut substrates, and ceramic or metal cylinders (e.g. to obtain targets for PLD or sputtering).

INFLRP: Peltier type cell PE120 for temperature range - 25 – 120 C has been used for temperature dependent measurement in THz spectroscopy

5. Difficulties Encountered in Implementing the Project

(a brief presentation of the difficulties and obstacles encountered that negatively affected the implementation of the project, proposed correction solutions).

First and foremost, we want to outline the big hurdles that our teams faced during the past year as result of the Covid-19 pandemic, which slowed down considerably the planned research activities, especially in the first half of 2020. The special circumstances caused by the Covid-19 pandemic, left many regions in Romania under hard lockdown (in particular, the Suceava county, were USV is located was the biggest Covid-19 hotspot in the country), and negatively impacted many of the research activities

planned to take place during the second year of the project. Therefore, some of the research activities had to be interrupted for a certain period, hiring has been curtailed, the access of researchers to the research facilities were forbidden or restricted, in-person meetings and reciprocal visits and exchange of researchers between the different teams had to be cancelled. To deal with this unprecedented situation, we had to tackle new challenges and the teams engaged in this project did their best to stay on track with the research activities although we had to quickly prioritize some tasks which seemed more feasible under the new conditions at the expense of others. Despite these obstacles, we are fully confident that in the next two years of the project all tasks and objectives will be accomplished to successfully complete the research project.

UAIC: Delay in arriving to the institution the funding corresponding to the current year, due to the delays in the national budget approval. Due to this, the salaries of the researchers with main position in the grants are received only in April-May. This makes difficult to maintain complete the grant research team. To mitigate this problem, I applied for support to my university, but they decided to pay only the taxes for the corresponding period and only later the remanent complete salaries. This makes each year difficult to keep young talented researchers in the grant team to work full time in research. The funds for young researchers should be separately ensured without any delays for the entire period, until the budget approval.

Date…….. **Project Manager**

22.02.2021 *(Name, Surname, Signature)*

Rotaru, Aurelian